SAND2017-9471R

International Collaboration on Spent Fuel Disposition in Crystalline Media: FY17 Progress Report

Fuel Cycle Research & Development

Prepared for
U.S. Department of Energy
Spent Fuel Waste Science & Technology
Yifeng Wang, Teklu Hadgu, Elena Kalinina,
Carlos Jove-Colon
Sandia National Laboratories
August 28, 2017
SFWD-SFWST-2017-000094

Sandia National Laboratories is a multi-mission laboratory managed and operated by National Technology and Engineering Solutions of Sandia, LLC., a wholly owned subsidiary of Honeywell International, Inc., for the U.S. Department of Energy's National Nuclear Security Administration under contract DE-NA0003525.

FCT Quality Assurance Program Document

Appendix E
FCT Document Cover Sheet

Name/Title of Deliverable/Milestone	International Collaboration on Spent Fuel Disposition in Crystalline Media: FY17 Progress Report (M4SF-17SN010302021)
Work Package Title and Number	DR Crystalline Disposal R&D
Work Package WBS Number	FT-17SN01030202
Responsible Work Package Manager	Yifeng Wang
	(Name/Signature)

Date Submitted 9/21/2016

Quality Rigor Level for Deliverable/Milestone	☐ QRL-3	☐ QRL-2	☐ QRL-1 ☐ Nuclear Data	☒ N/A*

This deliverable was prepared in accordance with Sandia National Laboratories
(Participant/National Laboratory Name)

QA program which meets the requirements of
☒ DOE Order 414.1 ☐ NQA-1-2000

This Deliverable was subjected to:

☐ Technical Review

Technical Review (TR)

Review Documentation Provided

☐ Signed TR Report or,
☐ Signed TR Concurrence Sheet or,
☐ Signature of TR Reviewer(s) below

Name and Signature of Reviewers

N/A

☐ Peer Review

Peer Review (PR)

Review Documentation Provided

☐ Signed PR Report or,
☐ Signed PR Concurrence Sheet or,
☐ Signature of PR Reviewer(s) below

*Note: In some cases there may be a milestone where an item is being fabricated, maintenance is being performed on a facility, or a document is being issued through a formal document control process where it specifically calls out a formal review of the document. In these cases, documentation (e.g., inspection report, maintenance request, work planning package documentation or the documented review of the issued document through the document control process) of the completion of the activity along with the Document Cover Sheet is sufficient to demonstrate achieving the milestone. QRL for such milestones may be also be marked N/A in the work package provided the work package clearly specifies the requirement to use the Document Cover Sheet and provide supporting documentation.

INTERNATIONAL COLLABORATION ON SPENT FUEL DISPOSITION IN CRYSTALLINE MEDIA: FY17 PROGRESS REPORT

EXECUTIVE SUMMARY

Active participation in international R&D is crucial for achieving the Spent Fuel Waste Science & Technology (SFWST) long-term goals of conducting "experiments to fill data needs and confirm advanced modeling approaches" and of having a "robust modeling and experimental basis for evaluation of multiple disposal system options" (by 2020). DOE's Office of Nuclear Energy (NE) has developed a strategic plan to advance cooperation with international partners. The international collaboration on the evaluation of crystalline disposal media at Sandia National Laboratories (SNL) in FY17 focused on the collaboration through the Development of Coupled Models and their Validation against Experiments (DECOVALEX-2019) project. The DECOVALEX project is an international research and model comparison collaboration, initiated in 1992, for advancing the understanding and modeling of coupled thermo-hydro-mechanical-chemical (THMC) processes in geological systems. SNL has been participating in three tasks of the DECOVALEX project: Task A. Modeling gas injection experiments (ENGINEER), Task C. Modeling groundwater recovery experiment in tunnel (GREET), and Task F. Fluid inclusion and movement in the tight rock (FINITO). The major accomplishments are summarized below:

- *Task A. Modeling gas injection experiments (ENGINEER):* Bentonite has been proposed as a buffer material for a deep geologic repository. Understanding gas migration in compacted clay materials is important for a performance assessment of an engineered barrier system of a repository system. Existing data demonstrate the complexity of gas migration in such low-permeability materials. Through a simple model analysis, we here show that this complexity can probably be explained with a bifurcation and chaos concept. The dynamic behavior of the system has been shown closely related to clay matrix dilation, fracturing and fracture healing as induced by gas bubble movement. The concept proposed here provide a new perspective for modeling gas migration in low-permeability materials.
- *Task C. Modeling groundwater recovery experiment in tunnel (GREET):* The task uses the data collected in a research tunnel at 500 m depth, at the Japan Atomic Energy Agency (JAEA) Mizunami Underground Research Laboratory (MIU), to understand the hydrological-mechanical-chemical environment. One of the objectives of Task C, Step 1, is to establish modeling methods and tools for analysis of excavation of tunnel. Fracture data analysis and preliminary modeling analysis have been carried out at SNL as part of Task C, Step 1. The fracture data analysis utilizes fracture data collected in the research tunnel and monitoring borehole 12MI33. A discrete fracture model has been developed based on fracture orientation, size and intensity derived from the fracture data analysis. The discrete model has been upscaled to an effective continuum model to be used in flow and transport simulations. A preliminary modeling analysis has also used project data to construct a simulation model to predict inflow into the inclined drift and the Closure Test Drift (CTD) during excavation.
- *Task F. Fluid inclusion and movement in the tight rock (FINITO):* Fluid inclusions can be found within mineral crystals or along grain boundaries in all types of sedimentary rocks. For a long-term performance assessment of a geologic repository, it is important

to characterize the distribution, amount and interconnectivity of fluid inclusions in the host rock and to predict migration of these inclusions after waste emplacement. Task F is designed to gain mechanistic understanding of possible physical processes involved in fluid inclusion migration in tight rocks such as rock salt or shale, with an ultimate goal to develop robust, predictive THMC modeling tools for a long-term performance assessment of a deep geologic repository in such media. The task will leverage the data provided by BGR, Germany. In fiscal year 2017, the work at SNL has focused on the model formulation of an individual fluid inclusion in rock salt. The model developed can qualitatively explain a number of key features of experimental observations. Specifically, the model can predict: (1) a linear increase in migration evelocity with increasing thermal gradient, (2) a nonlinear increase in migration velocity with inclusion size, (3) an overall aceleration in fluid migration with temperature, (4) the dependence of migration velocity on mechanical loadings. A preliminary analysis for biphase fluid inclusions has also been performed. A bifurcation point in vapor/liquid volume ratio for the direction of fluid migration is derived.

Future work will include the development of full models for gas migration in clay materials and fluid inclusion migration in salt. For Task C, more comprehensive modeling simulations will be conducted on fluid inflow and chemical reactions. For all three task, model simulation results will be closely compared to experimental and field data.

1. OBJECTIVES

Recognizing the benefits of international collaboration in the common goal of safely and efficiently managing the back end of the nuclear fuel cycle, DOE's Office of Nuclear Energy (NE) and its office for Spent Fuel Waste Science & Technology (SFWST) have developed a strategic plan to advance cooperation with international partners (Birkholzer et al., 2013; UFD, 2012). The plan lays out two interdependent areas of international collaboration. The first area is cooperation with the international nuclear community through participation in international organizations, working groups, committees, and expert panels. Such participation typically involves conference and workshop visits, information exchanges, reviews, and training and education. The second area of international collaboration is active R&D participation of U.S. researchers within international projects or programs (UFD, 2012). By active R&D, it is meant that U.S. researchers work closely together with international scientists on specific R&D projects relevant to both sides. With respect to geologic disposal of radioactive waste, such active collaboration provides direct access to information, data, and expertise on various disposal options and geologic environments that have been collected internationally over the past decades. Many international programs have operating underground research laboratories (URLs) in clay/shale, granite, and salt environments, in which relevant field experiments have been and are being conducted. Depending on the type of collaboration, U.S. researchers can participate in planning, conducting, and interpreting experiments in these URLs, and thereby get early access to field studies without having in situ research facilities in the United States.

The DOE also considers this second area, active international R&D, to be very beneficial in achieving the program's long-term goals of conducting "experiments to fill data needs and confirm advanced modeling approaches" and of having a "robust modeling and experimental basis for evaluation of multiple disposal system options" (by 2020). Advancing opportunities for active international collaboration with respect to geologic disposal has therefore been the primary focus of SFWST's international strategy in the recent year (Birkholzer et al., 2013; Birkholzer, 2012).

This report summarizes the work accomplished in FY17 at Sandia National Laboratories (SNL) related to international collaborations on the evaluation of crystalline rocks as disposal media. The FY17 work focused on the collaboration through the Development of Coupled Models and their Validation against Experiments (DECOVALEX-2019) project. The DECOVALEX project is an international research and model comparison collaboration, initiated in 1992, for advancing the understanding and modeling of coupled thermo-hydro-mechanical-chemical (THMC) processes in geological systems. SNL has been participating in three tasks of the DECOVALEX project: Task A. Modeling gas injection experiments (ENGINEER), Task C. Modeling groundwater recovery experiment in tunnel (GREET), and Task F. Fluid inclusion and movement in the tight rock (FINITO). This work directly supports the following SFWST objectives:

- Develop a fundamental understanding of disposal system performance in a range of environments for potential wastes that could arise from future nuclear fuel cycle alternatives through theory, simulation, testing, and experimentation.
- Develop a computational modeling capability for the performance of storage and disposal options for a range of fuel cycle alternatives, evolving from generic models to more robust models of performance assessment.

The work documented here also addresses the following specific topics identified based on the SFWST R&D Implementation Plan (Wang, 2014).

- Topic #S5: Evaluation of state of the art of site characterization techniques
- Topic #S7: Identification of the needs for using underground research laboratory
- Topic #P1: Development of discrete fracture network model
- Topic #P2: Parameter estimation and uncertainty quantification of field testing

1.1 REFERENCES

Birkholzer, J.T. (2012). Status of UFD Campaign International Activities in Disposal Research. Report prepared for U.S. Department of Energy Used Fuel Disposition Campaign, FCRD-UFD-2012-000295.

Birkholzer, J., Asahina, D., Chen, F., Gardner, P., Houseworth, J., Jove-Colon, C., Kersting, A., Nair, P., Nutt, M., Li, L., Liu, H.H., Painter, S., Reimus, P., Rutqvist, J., Steefel, C., Tynan, M., Wang, Y., Zavarin, M. (2013). An overview of US disposal research activities linked to international URLs. Proceedings of the 2013 International High-Level Radioactive Waste Management Conference (IHLRWM), April 28 – May 2, 2013, Albuquerque, New Mexico.

UFD (2012). Office of Used Fuel Disposition International Program — Strategic Plan (2013) April 2012, U.S. Department of Energy.

Wang, Y. (2014) Used Fuel Disposal in Crystalline Rocks: Status and FY14 Progress, FCRD-UFD-2014-000060.

2. FLUID INCLUSION AND MOVEMENT IN THE TIGHT ROCK (FINITO)

2.1 INTRODUCTION

Fluid inclusions containing liquid, gas or both phases can be found within mineral crystals (intra-crystalline) or along grain boundaries (inter-crystalline) in all types of sedimentary rocks (Roedder,1984; Ghanbaradeh et al., 2015). They were formed under various pressure and temperature conditions during the genesis. The size of fluid inclusions ranges several micrometres to millimeters and are usually invisible in detail without a microscope. These fluid inclusions are usually dispersed in a very low concentration but can form local accumulations in a rock volume up to some cubic meters.

The initial fluid inclusions in undisturbed rock are situated under a lithostatic pressure, which is much higher than a corresponding hydrostatic pressure in deep subsurface. Because of the low rock permeability, the migration of such fluids is almost impossible even under a high pressure-gradient condition. Fluid release from the crystal structure will take place if the stress state changes. In case of a drilling or an excavation, stress will be redistributed, resulting in a deviatoric stress state. If fluid pressure is higher than the minimal principal stress, dilatancy-controlled fluid migration occurs. This results in the generation of micro-fissures between crystal structures with an increased permeability. With regard to the long-term performance of a potential geologic repository, it is important to characterize the distribution, amount and interconnectivity of the fluid inclusions. It is also important to determine the permeability of micro-fissures and to characterize the hydraulic properties after the fluid release.

Understanding relevant underlying processes and developing appropriate model concepts are essential in this task. Modelling of the measured data needs a comprehensive effort, because a quantitative measurement at a microscale is not possible. An upscaling process from a microscale consideration to a macroscale observation is necessary.

In the construction phase of a geologic repository, coupled hydrologic-mechanical (HM) processes are important, while in the post-closure phase, coupled thermal-hydrologic-mechanical (THM) processes should be considered. In addition, chemical reactions and mineralogical alterations, especially under high temperature conditions, are indispensable to the full understanding of the system. The emphasis of this task is to gain understanding of possible physical processes involved in fluid inclusion migration in tight rocks such as rock salt or shale, with an ultimate goal to develop robust, predictive thermal-hydrologic-mechanical-chemical (THMC) modeling tools for a long-term performance assessment of a deep geologic repository.

2.2 EXPERIMENTAL DATA

Extensive microscopic study on the core structure using e.g. laser microscope, Computer tomography, electron backscatter diffraction (EBSD) is available which may help in description of the morphology of the pore space and construction of numerical mesh for the pore scale simulation. In addition, there are data about pressure, flow and geochemical components from

more than 20 boreholes from underground laboratories, which allow us to understand mechanical, hydraulic and geochemical processes (Hammer et al., 2013). Most of these data are provided by Federal Institute for Geosciences and Natural Resources (BGR), Germany.

2.3 PLAN FOR TASK CASE STUDY

Two cases are defined and will be qualitatively studied.

Case 1: Fluid migration due to excavation

In the operating phase of a repository, in a tight rock such as salt, embedded fluid inclusions may begin to move due to stress redistribution around the excavation and reopening of the micro-fissure and crystal boundary. The model system for this case is shown in Figure 2-1. We assume there is a fluid-inclusion in the tight rock located somewhere in a two-dimensional domain (10X10 m) constrained by an isotropic stress state of 25 MPa, indicating a depth of 1000 m below the surface. A hole with a diameter of 0.8 m will be drilled in the middle of the domain. Due to the excavation, fluid, may consist of two (gaseous and liquid) phase, begins to move towards to tunnel. Numerical tools are therefore needed to determine:

- the time-dependent stress redistribution due to mechanical creeping
- the zone with micro-fissure according to the dilatancy-criterion
- the shortest distance between the fluid inclusion and the drilled hole, which may induce to the movement of the fluid
- the percolation threshold for the fluid movement (capillary pressure, surface tension between three phases, minimal principal stress state).

In this case, a two-phase flow model coupled with a mechanical model (elastic, plastic and even creep model) is needed to analyze different scenarios even at the pore-scale domain.

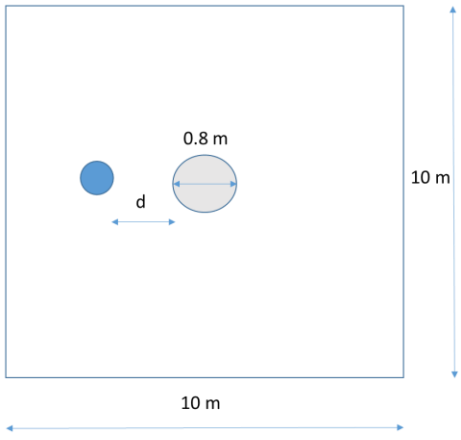

Figure 2-1: A single fluid inclusion located in a 2D domain with a hole.

Case 2: Fluid movement due to heating

In the closure phase of a repository, after the emplacement of the backfill, the stress state is approaching to the initial state. The micro-fissure will be healed again. However, under the high temperature conditions (100 – 200 °C) (Figure 2-2), thermal expansion of fluid and solid lead to volume increase. Due to the solubility difference, embedded fluid inclusions may move toward or away from a heating source (Figure 2-3).

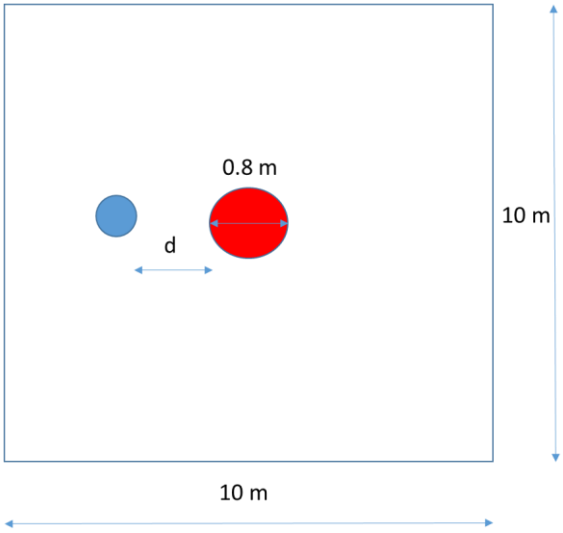

Figure 2-2: A single fluid inclusion located in a 2D domain with a heated domain.

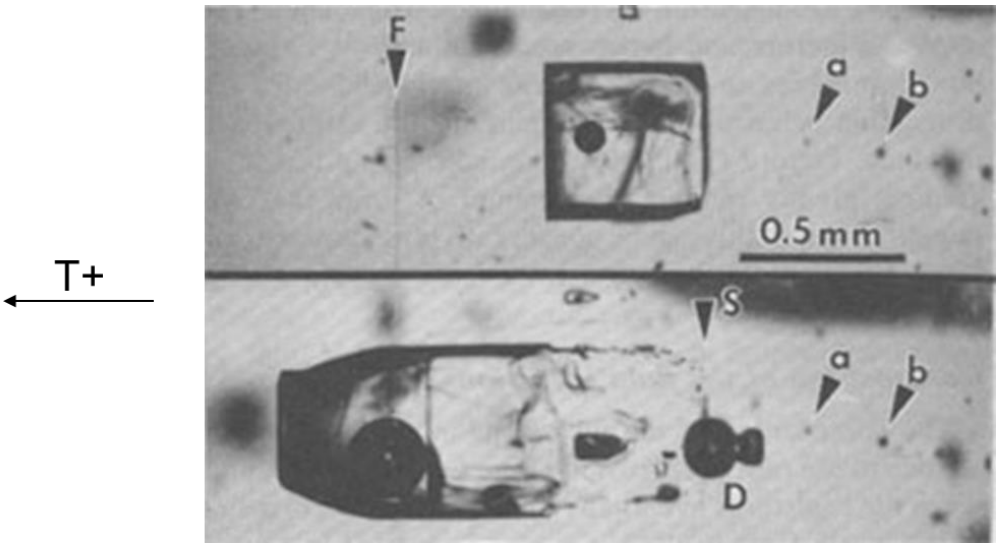

Figure 2-3: Experimental observation on fluid-migration after 156-hour run at 202°C ambient and 1.5°C/cm gradient (Roedder, 1984):

For this case, a coupled thermal-hydro-chemical model should be developed to consider all possible processes including:

- Mineral dissolution and precipitation on with a fluid inclusion
- Dihedral angle changes of fluid inclusion at grain boundaries,
- Thermal deformation,
- Induced porosity change and
- Related permeability change.

2.4 SCHEDULE

The master plan of the task includes three work packages with the focus on the understanding of the coupled thermal-hydro-mechanical and chemical processes involved in the system:

WP - 1: Literature study and process definition
WP - 2: Upscaling from microscale to macroscale basis
WP - 3: Model development and against observations

		2016		2017		2018		2019
	1 WS	2 WS	3 WS	4 WS	5 WS	6 WS	7 WS	8 WS
WP - 1								
Literature Recherche & Data Analyse								
Process Definition/Description								
Conceptuel Modeling								
WP - 2								
Upscalling Study (microscale - macroscale)								
Mathematical Formulation								
Programm Developement/Implement								
WP - 3								
Modelling against Observation								

2.5 MATHEMATICAL FORMULATION OF FLUID INCLUSION MIGRATION UNDER A THERMAL GRADIENT

In fiscal year 2017, the work at Sandia National Laboratories (SNL) has focused on the model formulation of an individual fluid inclusion in rock salt. A number of experimental and modelling studies have been conducted on fluid inclusion migration in salt (Anthony and Cline, 1971, 1972; Olander et al., 1981; Yagnik, 1983). A reasonable model should be able to account for the following key features of fluid inclusion migration observed experimentally (Figure 2-4):

- A liquid fluid inclusion moves toward a heating source at a velocity linearly proportional to the thermal gradient imposed (Figure 2-4A). Interestingly, it seems that the migration velocity also depends on a mechanical loading. Increasing the mechanical loading enhances migration.
- The velocity of inclusion migration also increases with the size of the inclusion, but not linearly (Figure 2-4B). The velocity appears to reach a plateau as the size of the inclusion further increases. This plateau seems to shift to a higher value at a higher temperature. This shift becomes more pronounced for small inclusions.

A

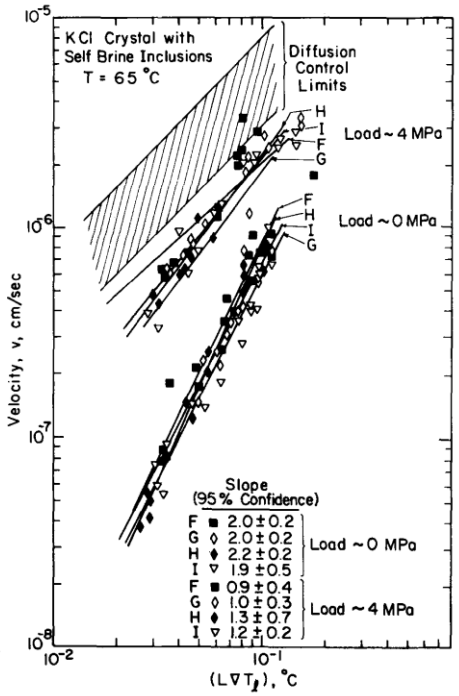
KCl Crystal with
Self Brine Inclusions
T = 65 °C
Diffusion
Control
Limits
H
I
F
G
Load ~ 4 MPa
F
H
I
G
Load ~ 0 MPa
Velocity, v, cm/sec
Slope
(95% Confidence)
F ■ 2.0±0.2
G ◊ 2.0±0.2
H ♦ 2.2±0.2
I ▽ 1.9±0.5
Load ~ 0 MPa
F ■ 0.9±0.4
G ◊ 1.0±0.3
H ♦ 1.3±0.7
I ▽ 1.2±0.2
Load ~ 4 MPa
(L∇T), °C

B

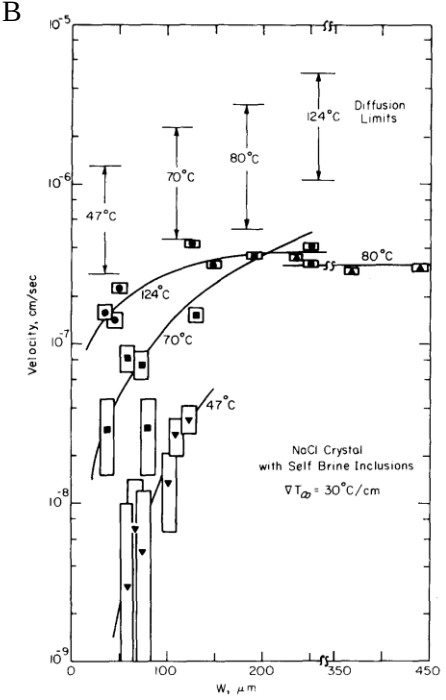
Diffusion
Limits
124°C
80°C
70°C
47°C
80°C
124°C
70°C
47°C
NaCl Crystal
with Self Brine Inclusions
Velocity, cm/sec
W, μm

C

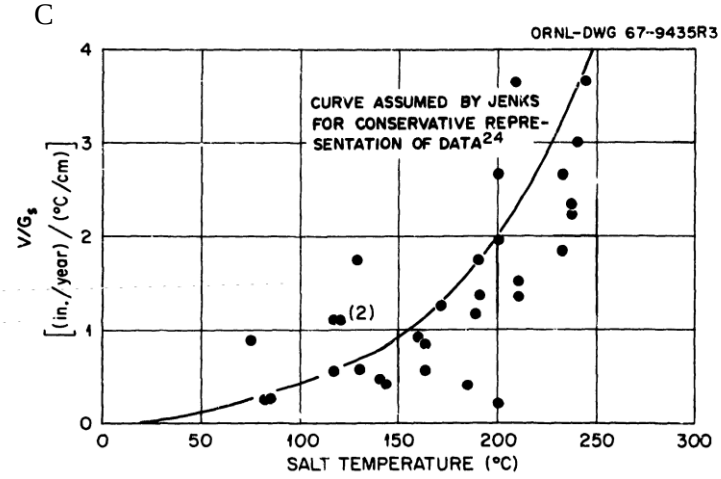
ORNL-DWG 67-9435R3
CURVE ASSUMED BY JENKS
FOR CONSERVATIVE REPRE-
SENTATION OF DATA[24]
(2)
V/G_s
[(in./year)/(°C/cm)]
SALT TEMPERATURE (°C)

D

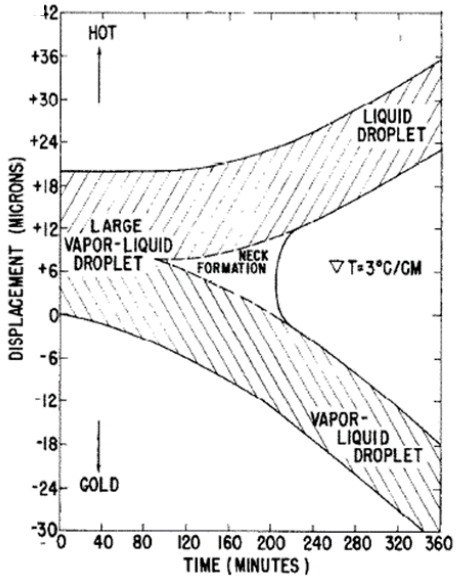
HOT
LIQUID
DROPLET
LARGE
VAPOR-LIQUID
DROPLET
NECK
FORMATION
∇T=3°C/CM
VAPOR-
LIQUID
DROPLET
COLD
DISPLACEMENT (MICRONS)
TIME (MINUTES)

E

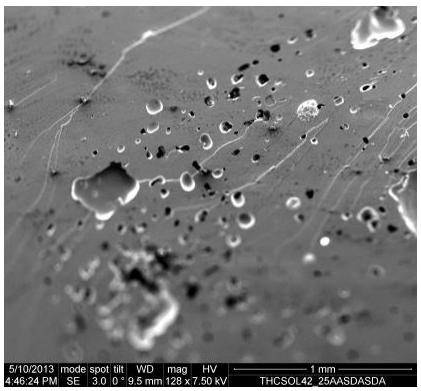
5/10/2013 mode spot tilt WD mag HV 1 mm
4:46:24 PM SE 3.0 0 ° 9.5 mm 128 x 7.50 kV THCSOL42_25AASDASDA

F

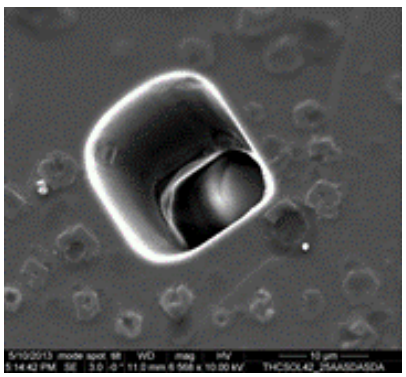

Figure 2-4: Key features of fluid inclusion migration under a thermal gradient. A – C: Migration velocity of liquid inclusion as a function of temperature gradient, inclusion size, and temperature (Olander et al., 1982; Jenk, 1979). D: Liquid-dominated inclusions migrate upward the thermal gradient while vapour-dominated inclusions move downward the gradient (Anthony and Cline, 1972); E-F: Channelling of an advancing front of a moving fluid inclusion (F. Caporuscio, per. Comm.), indicating the morphologic instability of the front.

- The velocity of fluid inclusion migration increases approximately exponentially with the overall temperature (Figure 2-4C).
- Complex behaviours have been observed for biphase inclusions. Liquid-dominated inclusions migrate upward the thermal gradient while vapour-dominated inclusions move downward the gradient (Figure 2-4D). Therefore, there is a bifurcation point in a vapour/liquid ratio for the direction of inclusion movement.
- As a fluid inclusion migrate along a thermal gradient, its shape may change and it may break into smaller inclusions (Yagnik, 1983). Remarkably, at the advancing front of an inclusion, channelling may be developed, indicating morphologic instability of the front (Figures 2-4E and 2-4F).

To account for these feature, we have formulated the following dynamic model for a single fluid inclusion migration in a thermal gradient field.

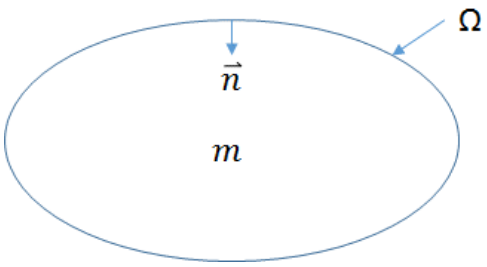

Figure 2-5: Modeling system for single inclusion migration in a thermal gradient field.

The modeling system is shown in Figure 2-5. A liquid-phase fluid inclusion enclosed in a closed surface Ω. We assume that the mass transfer within the inclusion can be described with a molecular diffusion process and that the thermal gradient within the inculsion is approxiamtely identail to the ambent gradient. Wthin Ω, we have:

$$\frac{\partial m}{\partial t} = D\nabla^2 m \qquad (2\text{-}1)$$

$$\frac{\partial T}{\partial x} = \alpha \qquad (2\text{-}2)$$

where m is the concentration of dissolved salt; D is the diffusion coefficient; T is the temperature; α is the thermal gradient; x is the coordination along the impose thermal gradeint; and t is the time.

On the inner surface Ω, mineral dissolution and precipitation takes place:

$$NaCl(s) \leftrightarrow NaCl(aq).$$

The mass balance on the surface can be described by:

$$R_d = k(K_d - m) \tag{2-3}$$

$$K_d(T,\ \kappa) = K_d^0 e^{\frac{\Delta H_r}{RT}\left(\frac{T}{T_0}-1\right)-\frac{2\gamma V_m \kappa}{RT}} \tag{2-4}$$

$$-D\vec{\nabla}m \cdot \vec{n} = R_d \tag{2-5}$$

where R_d is the mineral dissolution rate; K_d is the solubility of the mineral; k is the reaction rate constant; T_0 is the temperature at the center of the inclusion; K_d^0 is the mineral solubility at temperature T_0; ΔH_r the enthalpy of the mineral dissolution reaction; γ is the surface energy of the solution-salt interface; V_m is the molar volume of the salt; κ is the curvature of the surface; R is the gas constant; and $\vec{n}$ is the unit normal vector pointing inward (see Figure 2-5).

The evolution of inclusion surface can be described by the following kinematic equations (Wang and Merino, 1995):

$$\Omega(x, y, z, t) = 0 \tag{2-6}$$

$$\vec{\nabla}\Omega \cdot \vec{V} + \frac{\partial \Omega}{\partial t} = 0 \tag{2-7}$$

$$\vec{V} + V_0\vec{\imath} = -V_m R_d \vec{n} \tag{2-8}$$

$$\vec{n} = -\frac{\vec{\nabla}\Omega}{|\vec{\nabla}\Omega|} \tag{2-9}$$

$$\kappa = -\vec{\nabla} \cdot \vec{n} \tag{2-10}$$

where V_0 is the velocity of fluid inclusion migration; and $\vec{V}$ is the velocity of inclusion surface movement relative to the center of the inclusion. Equations (2-1) to (2-10) constitute a moving boundary problem for single fluid inclusion migration along a thermal gradient. This set of equations can be solved using a level-set method.

2.6 PRELIMINARY MODEL ANALYSIS

A first-order analysis has been conducted based on the model developed above. For a spherical liquid inclusion with a radius r, and assuming $k \to \infty$, the velocity of inclusion migration under a thermal gradient α can be estimated by:

$$V_0 \approx \frac{V_m D K_d^0 \Delta H_r \alpha}{R T_0^2} e^{-\frac{2\gamma V_m}{R T_0 r}} . \qquad (2\text{-}11)$$

This simple equation can qualitatively explain the following key features experimentally observed:

- The model predicts a linear increase in migration evelocity with increasing thermal gradient α, as observed (Figure 2-4A).
- The model predicts that, as the size of the inclusion increases, the velocity of inclusion migration increases and then approaches a plateau. Also, as the temperature increases, the surface energy γ is expected to decrease (Ghanbaradeh et al., 2015), thus shifting the plateau upward. Furthermore, as the size of the inclusion decreases, the migration velocity diminishes. All these predictions are qualitatively consistent with the observations (Figure 2-4B).
- Both terms D and K_d^0 in equation (2-11) expeonentailly increase with temperature. At elevated temperatures, the two terms are expected to take over the term T_0^2 in the denominator in the equation, leading to an overall exponential increase in migaration velocity with temperature, as shown in Figure 2-4C.
- Since the solubility of a mineral depends on the stress to which the mineral is subjected (Wang, 2016). A high mechanical loading results in a higher solubility of the mineral, therefore acelerating inclusion migration (Figure 2-4A).

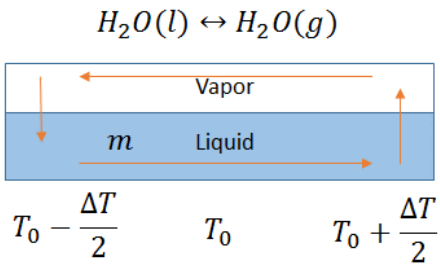

Figure 2-6: A simplified representation of a biphase fluid inclusion, in which a continuous vapor-liquid conversion takes place along a thermal gradient.

Simiarly, a preliminary analysis for biphase fluid inclusions has also been performed. For simplicity, a simple geometry of a fluid inclusion is assumed as shown in Figure 2-6. The mass continuity equations for both vapor and liquid as well as for the dissolved salt can be described by:

$$\rho_v(T) = \rho_v^0 e^{\frac{\Delta H_r^W}{RT}\left(\frac{T}{T_0}-1\right)} \quad (2\text{-}12)$$

$$A_v D_v \frac{\partial \rho_v}{\partial x} = A_l V_l \rho_w \quad (2\text{-}13)$$

$$-D\frac{\partial m}{\partial x} + mV_l = 0 \quad (2\text{-}14)$$

where ρ_v^0 is the vapor density at temperarture T_0; $\rho_v(T)$ is the vapor density at temperature T; ρ_w is the density of the liquid; ΔH_r^W is the enthalpy of liquid-vapor phase transition; A_v and A_l are the cross section areas of vapor and liquid respectively; D_v is the diffusion coefficient of vapor; and V_l is the local flow velocity of liquid. Assuming that the reaction rate for salt dissolution and precipitation $k \to \infty$, we obtain the bifurcation point in vapor/liquid volume ratio ($f = \frac{A_v}{A_l}$) for fluid inclusion migration:

$$f_c = \frac{D\Delta H_r \rho_w}{D_v \Delta H_r^W \rho_v^0(T_0)} \quad (2\text{-}15)$$

When $f > f_c$, the inclusion tends to move away from the heating surface, while for $f < f_c$, the inclusion tends to move upward the thermal gradient.

2.7 SUMMARY

Fluid inclusions can be found within mineral crystals or along grain boundaries in all types of sedimentary rocks. For a long-term performance assessment of a geologic repository, it is important to characterize the distribution, amount and interconnectivity of fluid inclusions in the host rock and to predict migration of these inclusions after waste emplacement. DECOVALEX Task F is designed to gain mechanistic understanding of possible physical processes involved in fluid inclusion migration in tight rocks such as rock salt or shale, with an ultimate goal to develop robust, predictive THMC modeling tools for a long-term performance assessment of a deep geologic repository in such media. The task will leverage the data provided by BGR, Germany. In fiscal year 2017, the work at SNL has focused on the model formulation of an individual fluid inclusion in rock salt. The model developed can qualitatively explain a number of key features of experimental observations. Specifically, the model can predict: (1) a linear increase in migration evelocity with increasing thermal gradient, (2) a nonlinear increase in migration velocity with inclusion size, (3) an overall aceleration in fluid migration with temperature, (4) the dependence of migration velocity on mechanical loadings. A preliminary analysis for biphase fluid inclusions has also been performed. A bifurcation point in vapor/liquid volume ratio for the direction of fluid migration is derived.

2.8 REFERENCES

Anthony, T. R. and Cline, H. E. (1971) Thermal migration of liquid droplets through solids, J. Applied Physics, 42, 3380-3387.

Anthony, T. R. and Cline, H. E. (1972) The thermomigration of biophase vapor-liquid droplets in solids, Acta Metallurgica, 20, 247-255.

Ghanbarzadeh, S., Hesse, M. A., Prodanović, M., Gardner, J. E. (2015) Deformation-assisted fluid percolation in rock salt, Science, 250, 1069-1072.

Hammer, Jörg, Pusch, Maximilian, Häger, Andreas, Scheeder, Georg, Shao, Hua, Paul, Benjamin, Ostertag-Henning, Christian, Mingerzahn, Gerhard, Schlömer, Stefan, Hesser, Jürgen (2013) Untersuchungen von Kohlenwasserstoffen im Erkundungsbergwerk Gorleben, BGR-Report, 2013.

Jenks, G. H. (1979) Effects of Temperature, Temperature Gradients, Stress, and Irradiation on Migration of Brine Inclusions in a Salt Repository, Oak Ridge National Laboratory, ORNL-5526.

Olander, D. R., Machiels, A. J., Balooch, M., Yagnik, S. K. (1982) Thermal gradient migration of brine inclusions in synthetic alkali halide single crystals, J. Applied Physics, 53, 669-681.

Roedder, E. (1984) The fluids in salt, American Mineralogist, 69, 413-439.

Wang, Y. (2016) On Subsurface fracture opening and closure, J. Petroleum Sci. Eng., 155, 46-53.

Wang, Y. and Merino, E. (1995) Origin of fibrosity and banding in agates from flood basalts, Am. J. Sci., 295, 49-77.

Yagnik, S. K. (1983) Interfacial stability of migration brine inclusions in alkali halide single crystals supporting a temperature gradient, J. Crystal Growth, 62, 612-626.

3. MODELLING GAS INJECTION EXPERIMENTS (ENGINEER)

3.1 INTRODUCTION

Rodwell et al. (1999) state "there are few problems in geoscience more complex than the quantitative prediction of gas migration fluxes through an argillaceous rock formation". To understand this statement, it is necessary to appreciate why clays and mudrocks differ from other clastic sedimentary rocks. Key factors in this respect include the sub-microscopic dimensions of the interparticle spaces, the very large specific surface of the mineral phases, strong physico-chemical interactions between water molecules and surfaces, very low permeability, generally low tensile strength, a deformable matrix, and a very pronounced coupling between the hydraulic and mechanical response of these materials. It is therefore necessary to consider these properties when defining the behavior of these materials in order to successfully represent flow in such systems.

With this in mind, the processes governing the movement of repository gases through engineered barriers and argillaceous host rocks can be split into two components, (i) molecular diffusion (governed by Fick's Law) and (ii) bulk advection. In the case of a repository for radioactive waste based on a generic KBS-3 concept, corrosion of metallic materials under anoxic conditions will lead to the formation of hydrogen. Radioactive decay of the waste and the radiolysis of water are additional source terms. If the rate of gas production exceeds the rate of gas diffusion within the pores of the barrier or host rock, a discrete gas phase will form (Weetjens and Sillen, 2006; Ortiz et al., 2002; Wikramaratna et al., 1993). Under these conditions, gas will continue to accumulate until its pressure becomes sufficiently large for it to enter the surrounding material.

In clays and mudrocks, four primary phenomenological models describing gas flow can be defined, Figure 3-1: (1) gas movement by diffusion and/or solution within interstitial fluids along prevailing hydraulic gradients; (2) gas flow in the original porosity of the fabric, commonly referred to as viscocapillary (or 2-phase) flow; (3) gas flow along localised dilatant pathways, which may or may not interact with the continuum stress field; and (4) gas fracturing of the rock similar to that performed during hydrocarbon stimulation exercises.

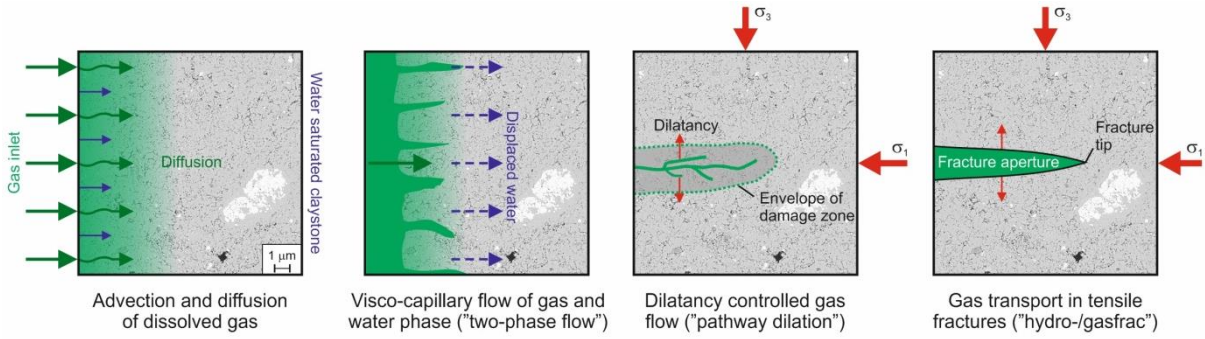

Figure 3-1: *Conceptual models of gas flow.*

There is now a growing body of evidence (Horseman et al., 1999, 2004; Harrington and Horseman, 1999; Angeli et al., 2009; Harrington et al., 2009) that in the case of plastic clays and in particular bentonite, classic concepts of porous medium two-phase flow are inappropriate and continuum approaches to modelling gas flow may be questionable, depending on the scale of the processes and resolution of the numerical model. However, the detail of the dilatant mechanisms controlling gas entry, flow and pathway sealing are unclear and the "memory" of such features within clay may impair barrier performance, in particular, acting as preferential flow paths for the movement of radionuclides.

As such, development of new and novel numerical representations for the quantitative treatment of gas in clay-based repository systems are therefore required, and are the primary focus of this Task. These will provide an invaluable tool with which to assess the impact of gas flow on repository layout and therefore design of any future facility. In addition, the same processes and mechanisms described in such models are of direct relevance to other clay-based engineering issues where immiscible gas flow is involved e.g. shale gas, hydrocarbon migration, carbon capture and storage and landfill design. The Task is split into a number of stages each building on the previous, representing an incremental increase in complexity. For each stage a specific experiment(s) will be presented and a series of constraints, variables and metrics stated in order to adequately define the scope of the Task.

Activity	Spring 2016	Autumn 2016	Spring 2017	Autumn 2017	Spring 2018	Autumn 2018	Spring 2019	Autumn 2019
Stage 0: code development								
Stage1 A & B: 1D flow (laboratory)								
Stage 2 A & B: Spherical flow (laboratory)								
Interim reporting								
Stage 3A: Gas flow in natural clay								
Stage 3B: Gas flow in pelletised bentonite								
Final Reporting								

3.2 NONLINEAR DYNAMICS OF GAS MIGRATION IN COMPACTED CLAY

In fiscal year 2017, the work at Sandia National Laboratories (SNL) has emphasized on the conceptual model development for gas migration in compacted clay materials. The model focuses on the nonlinear dynamic aspects of the process observed in experiments. As shown in Figure 3-2, gas migration in a water saturated compacted clay material exhibits rich nonlinear dynamic behaviours as the injection gas pressure varies: from a constant out flow to a periodic outflow and eventually to a chaotic behaviour. To test if the outflow variation is truly chaotic, we have plotted a segment of outflow curve in an embedded space [see the method in Strogatz (2001)]. It can be seen in Figure 3-3 that in the embedded space the outflow seems to possess an internal structure, i.e., not completely random (white noise), indicating a possible chaotic behavior.

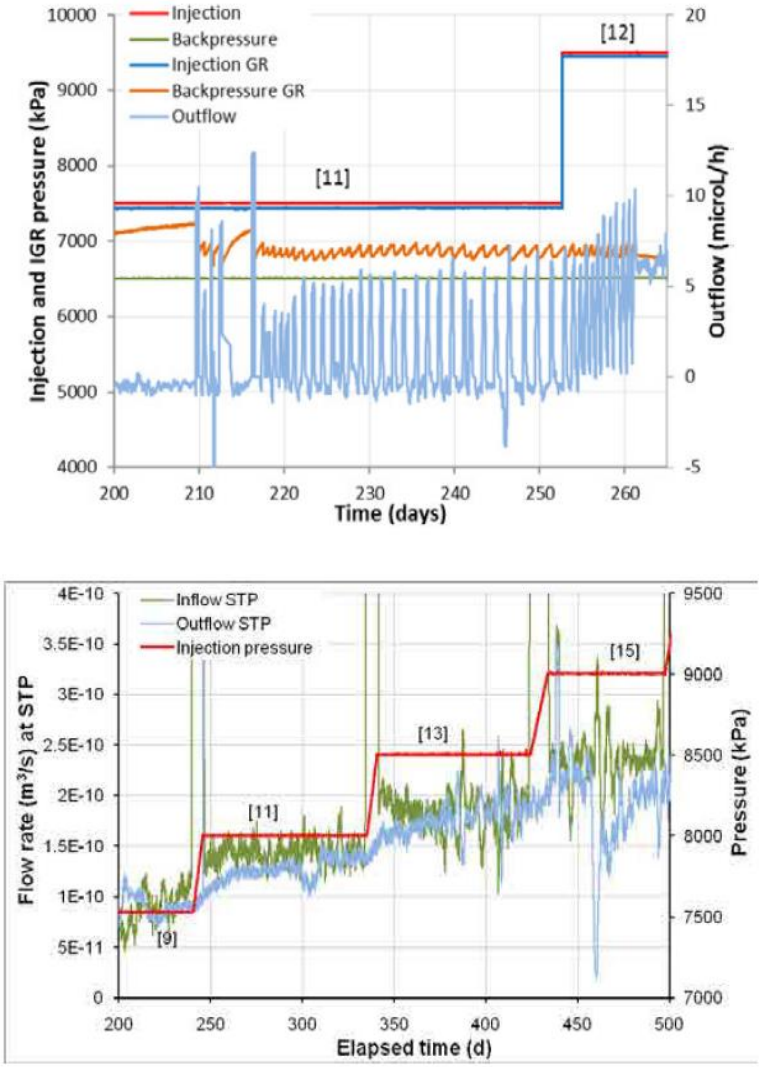

Figure 3-2: Nonlinear behaviors of gas migration in water saturated compacted clay materials (Cuss et al., 2012).

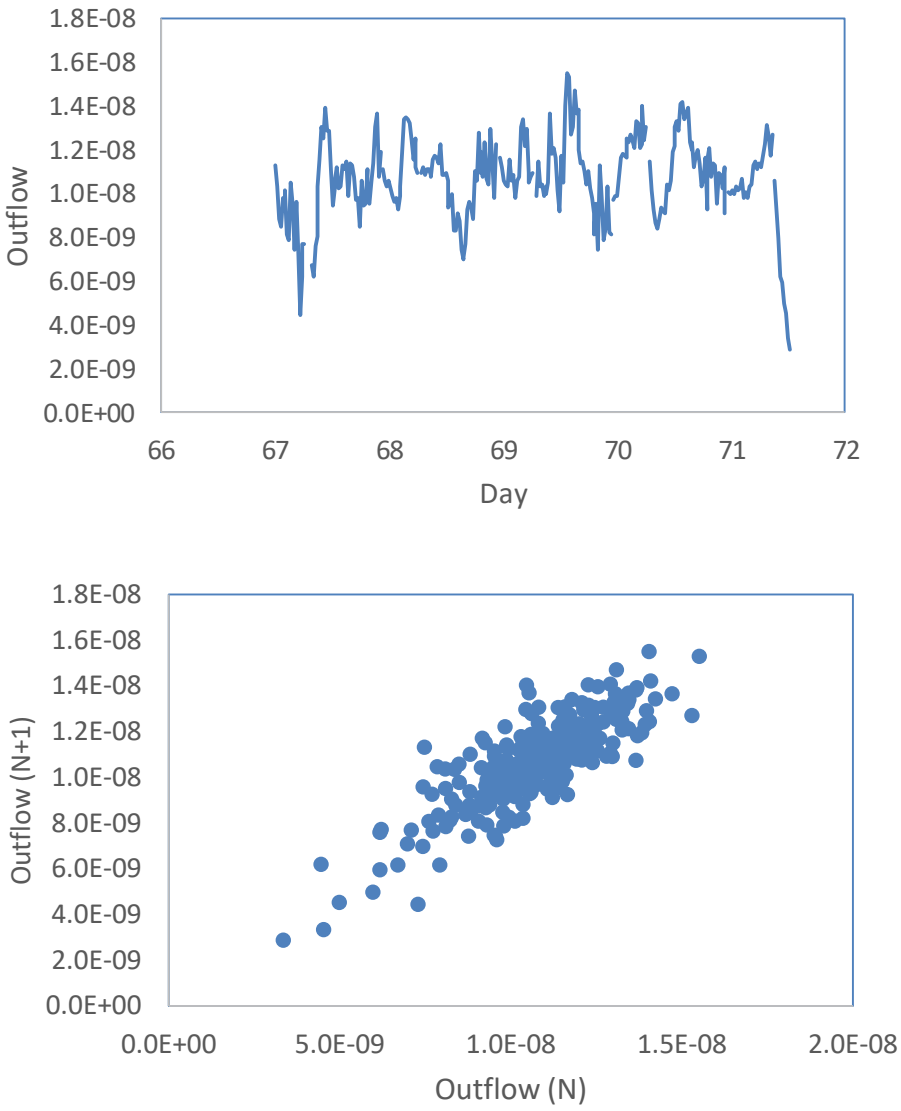

Figure 3-3: Outflow behavior in an embedded space. A: Original data; B: Outflow in an embedded space.

To explain these dynamic behaviors, we have developed a chaotic model based on the concept of delay logistic model (Strogatz, 2001; Bani-Yaghoub, 2017). For illustration, we focus on single gas bubble movement in a compacted clay material under a gas pressure gradient (Figure 3-4). The underlying assumption is that, given a low permeability of the material, the dominant mechanism for gas migration is first to form a bubble nucleation and then to push the bubble through the clay matrix through matrix dilation and fracturing. In the wake of bubble movement, matrix compression and fracture healing may also take place. With this assumption, the evolution of mass and pressure within a bubble of a volume V can simply expressed by:

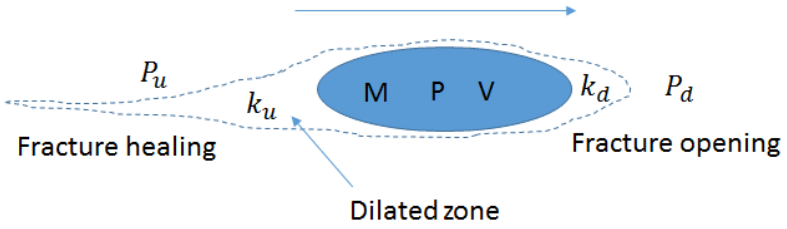

Figure 3-4: Conceptual model for gas bubble movement in a compact clay material under a pressure gradient.

$$\frac{dM}{dt} = k_u(P_u - P) - k_d(P - P_d) \quad (3\text{-}1)$$

where M is the gas mass in the bubble; P is the gas pressure in the bubble; P_u and P_d are the gas pressures in the upstream and the downstream of the bubble movement respectively; k_u and k_d are the permeability of the matrix in the upstream and the downstream of the bubble movement respectively; and t is the time. Considering a possible effect of dilation, fracturing and fracture healing on matrix permeability, we assume that k_u and k_d are proportional to the gas pressure P:

$$k_u = k_u^0 P \quad (3\text{-}2)$$

$$k_d = k_d^0 P \quad (3\text{-}3)$$

where k_u^0 and k_d^0 are constant. With the ideal gas law $M = \frac{PV}{RT}$, where R is the gas constant and T is the temperature, the equation (3-1) can be cast into:

$$\frac{dP}{dt} = \lambda_1 P\left(1 - \frac{P}{K}\right) \quad (3\text{-}4)$$

Equation (3-4) is a continuous logistic equation, with

$$\lambda_1 = \frac{(k_u^0 P_u + k_d^0 P_d)RT}{V} \quad (3\text{-}5)$$

$$\lambda_2 = \frac{(k_u^0 + k_d^0)RT}{V} \quad (3\text{-}6)$$

$$K = \frac{\lambda_1}{\lambda_2}. \quad (3\text{-}7)$$

As discussed above, clay matrix may have a memory effect on deformation and fracturing, which implies that the permeabilities k_u and k_d depends not only on the current pressure value but also the recent history of the pressure, which can be captured by the following delay logistic equation:

$$\frac{dP}{dt} = \lambda_1 \left(1 - \frac{P}{K}\right) \int_{-\infty}^{t} G(t-s)p(s)ds \qquad (3\text{-}8)$$

where $G(t)$ is a kernel function characterizing the influence of the pressure at a previous step on the permeability at the current time step. A commonly chosen kernel function is an exponential function characterizing an exponential decay of the influence as the time interval increases:

$$\frac{dP}{dt} = \lambda_1 \left(1 - \frac{P}{K}\right) \int_{-\infty}^{t} \alpha e^{-\alpha(t-s)} p(s)ds. \qquad (3\text{-}9)$$

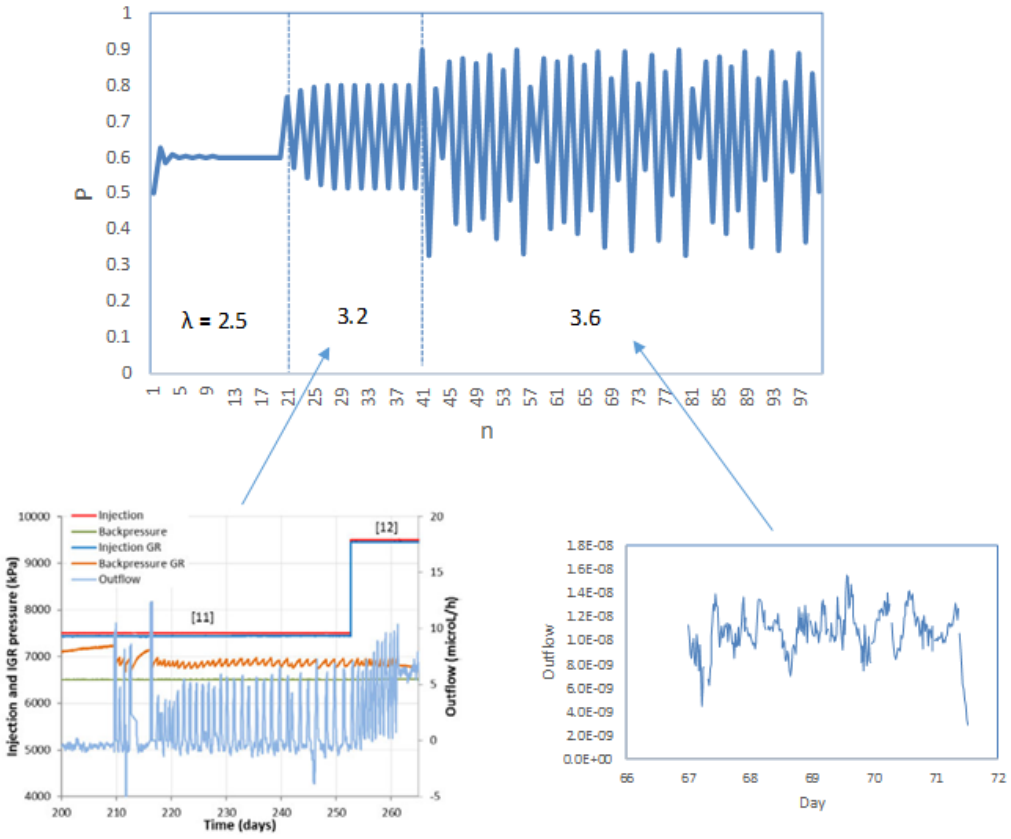

Figure 3-5: Explanation of gas migration dynamics from a chaotic point of view. Experimental measurements are from Cuss et al. (2012).

For an illustration of the concept of bifurcation and chaos for gas migration, let's assume the gas movement is more or less stepwise. Equation (3-4) can then be reduced to a logistic map:

$$p_{n+1} = \lambda p_n(1 - p_n) \quad (3\text{-}10)$$

with

$$\lambda = 1 + \lambda_1 \Delta t \quad (3\text{-}11)$$

where is a scaled gas pressure inside the bubble. It is known that Equation (3-10) can exhibit rich dynamic behaviors (Strogatz, 2001) as shown in Figure 3-5.

3.3 SUMMARY

Bentonite has been proposed as a buffer material for a deep geologic repository. Understanding gas migration in compacted clay materials is important for a performance assessment of an engineered barrier system of a repository system. Existing data demonstrate the complexity of gas migration in such low-permeability materials. Through a simple model analysis, we here show that this complexity can probably be explained with a bifurcation and chaos concept. The dynamic behavior of the system has been shown closely related to clay matrix dilation, fracturing and fracture healing as induced by gas bubble movement. The concept proposed here provide a new perspective for modeling gas migration in low-permeability materials.

3.4 REFERENCES

Angeli, M., Soldal, M., Skurtveit, E. and Aker, E. (2009) Experimental percolation of supercritical CO_2 through a caprock. Energy Procedia,1, 3351-3358.

Bani-Yaghoub, M. (2017) Analysis and applications of delay differential equations in biology and medicine, arXiv:1701.04173v1.

Cuss, R. J., Harington, J. F., and Noy, D. J. (2012) Final Report of FORGE WP4.1.1: Stress-Path Permeameter Experiment Conducted on Callovo-Oxfordian Claystone, British Geological Survey, Minerals and Waste Programme Commissioned CR/12/140.

Harrington, J.F. and Horseman, S.T. (1999). Gas transport properties of clays and mudrocks. In: Muds And Mudstones: Physical And Fluid Flow Properties (eds A.C.Aplin, A.J. Fleet, and J.H.S. Macquaker). Geological Society of London, Special Publication No. 158, 107-124.

Horseman, S.T., Harrington, J.F. and Sellin, P. (1999). Gas migration in clay barriers. Engineering Geology, Vol. 54, 139-149.

Horseman, S.T., Harrington, J.F. and Sellin, P. (2004) Water and gas flow in Mx80 bentonite buffer clay. In: Symposium on the Scientific Basis for Nuclear Waste Management XXVII (Kalmar), Materials Research Society, Vol. 807. 715-720.

Harrington, J.F., Noy, D.J., Horseman, S.T., Birchall, J.D. and Chadwick, R.A. (2009) Laboratory study of gas and water flow in the Nordland Shale, Sleipner, North Sea. Pp. 521-543 in:

Carbon Dioxide Sequestration in Geological Media State of the Science (M. Grobe, J.C. Pashin and R.L. Dodge, editors). AAPG Studies in Geology, 59. American Association of Petroleum Geologists, Tulsa, Oklahoma, USA.

Ortiz, L., Volckaert, G. and Mallants, D. (2002) Gas generation and migration in Boom Clay, a potential host rock formation for nuclear waste storage. Engineering Geology, 64, 287-296.

Rodwell W R, Harris A W, Horseman S T, Lalieux P, Müller M, Ortiz Amaya L, Pruess K, 1999. Gas migration and two-phase flow through engineered and geological barriers for a deep repository for radioactive waste. EC/NEA Status Report EUR 19122EN, European Union, Luxembourg.

Strogatz, S. H. (2001) Nonlinear Dynamics and Chaos: With Applications to Physics, Biology, Chemistry, and Engineering, Westview.

Weetjens, E. and Sillen, X. (2006) Gas Generation and Migration in the Near Field of a Supercontainer-Based Disposal System for Vitrified High-Level Radioactive Waste. Proceedings of the 11th International High-Level Radioactive Waste Management Conferance (IHLRWM), Las Vegas, Nevada, USA.

Wikramaratna, R.S., Goodfield, M., Rodwell, W.R, Nash, P.J. and Agg, P.J. (1993) A Preliminary Assessment of Gas Migration from the Copper/Steel Canister. SKB Technical report TR93-31. Swedish Nuclear Fuel and Waste Management Company (SKB), Stockholm, Sweden.

4. MODELING GROUNDWATER RECOVERY EXPERIMENT IN TUNNEL (GREET)

4.1 INTRODUCTION

The major goal of this study was developing fracture model of the granite rocks for the area surrounding the MIU research tunnel at 500 m depth. The fracture model is needed for simulation of hydrogeologic and geochemical conditions in the various experiments being conducted in the research tunnel as a part of GREET (Groundwater REcovery Experiment in Tunnel) project.

The modeling domain is 100x150x100m with the main experimental part of the tunnel, Closure Test Drift (CTD), located approximately in the center. The majority of model is within the lower sparsely fractured domain (LSFD) of the Toki granite. Figure 4-1 shows the modeling domain, the research tunnel (CTD and Inclined Drift), the horizontal monitoring borehole 12MI33 (with 6 test intervals), and the vertical exploratory borehole MIZ-1 (only 2 test intervals are inside the modeling domain).

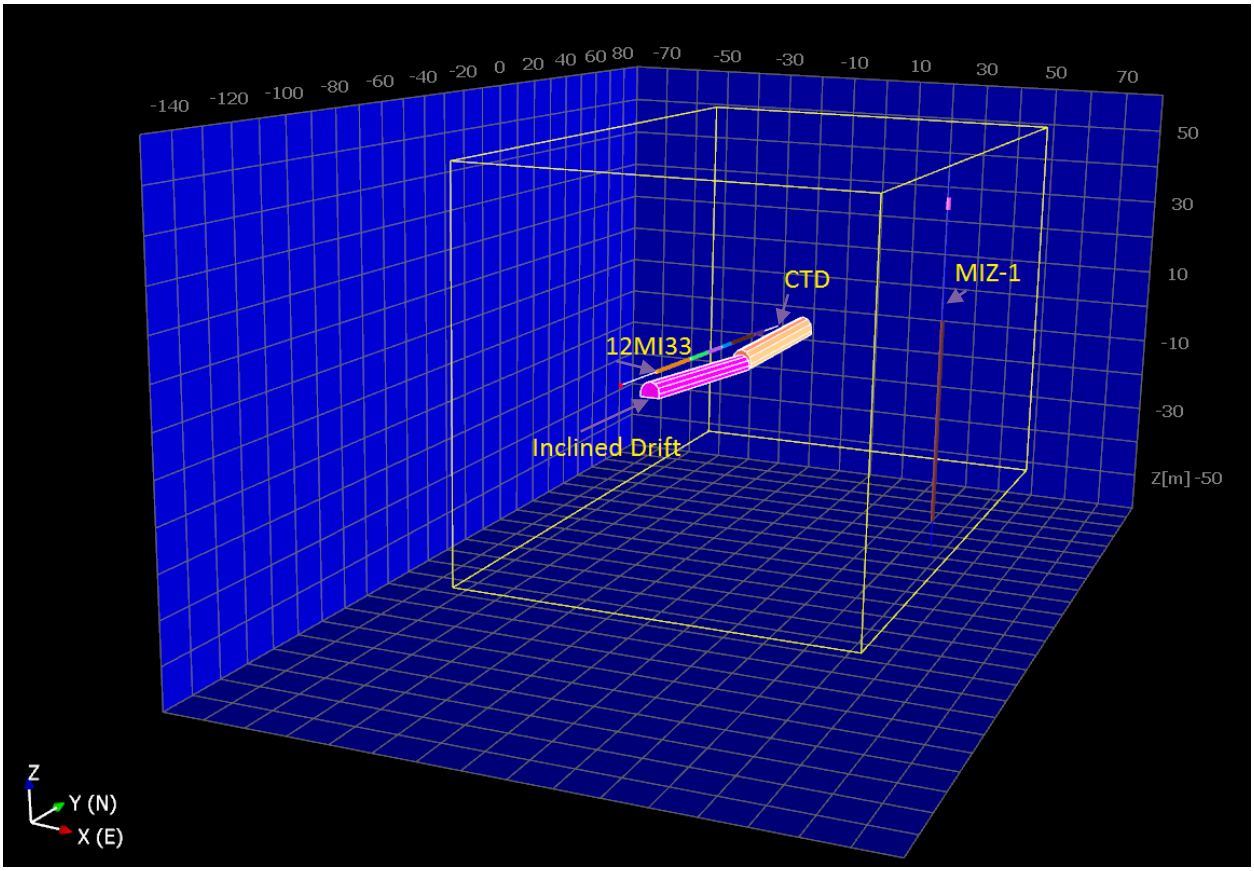

Figure 4-1: Modeling Domain and Location of Research Tunnel and Boreholes.

The following data were used in the fracture analysis:

- Fractures traces on the walls of CTD, Inclined Drift, and Access Drift. Note that Access drift fracture data were used in the analysis even though this drift is outside the modeling domain.
- Fractures observed in borehole 12MI33.
- Packer test data in 6 test intervals of 12MI33 and 2 test intervals of borehole MIZ-1.
- Measured inflow into the research drift.

The goal of the fracture analysis was to estimate fracture orientation, size and intensity and use these estimates to develop discrete fracture model (DFN). The DFN model is then converted to an equivalent continuum model with the grid cell size 1x1x1 m (1,500,000 grid blocks) using Oda's method [Ref. 1]. Multiple realizations of DFN and corresponding equivalent continuum model will be used to simulate groundwater flow and transport in vicinity of the research tunnel. The developing of DFN is demonstrated using one realization as an example. Fracman (Golder software, Ref. 1) was used to develop the model.

4.2 GENERATING FRACTURES USING RESEARCH TUNNEL FRACTURE TRACE DATA

2,023 fractures were observed on the wall of the research tunnel. The fracture trace data include trace segment coordinates, length, dip, strike, alteration (if any), and flow range (if any). 146 fractures (7.2%) selected for the analysis are the fractures with an observed flow (Table 1). These fractures are described in the original data based on the flow range as "flow" (F) fractures (>1L/min), "dripping" (D) fractures (<0.1L/min), and "wet" (W) (<0.1L/min).

Table 4-1. Research Tunnel Fractures Included in the Fracture Analysis.

Research Tunnel Area	**F-Fractures** (flow>1.0 L/min)	**D-Fractures** (flow<0.1 L/min)	**W-Fractures** (flow<0.1 L/min)
CTD	4	15	3
Inclined Drift	14	42	N/A
Access Drift	N/A	65	3
Total	**18**	**122**	**6**

The trace data were imported into the model and are shown in Figure 4-2. The trace length analysis was conducted separately for F-; D-; and W- fractures. Fracman uses algorithm described in Ref. 2 and 3 to estimate fracture size (equivalent radius) from the trace length distribution. The trace length distributions of all 3 sets are best described with the lognormal distributions. The distributions of W- and D- fractures are very similar and were combined in one. The power law distributions, that are often used for fracture radius, were found to be not a good fit to these data. The equivalent fracture radius distributions estimated from the trace length data are summarized in Table 4-2. The F fractures with greater flow rates are also the ones with the larger size. This is consistent with the common concept according to which the fracture transmissivity and aperture are positively correlated with the fracture radius.

Table 4-2. Equivalent Fracture Radius Distribution Parameters.

Fracture Set	Distribution Type	Mean Radius (m)	Standard Deviation (m)
D- and W-Fractures	Lognormal	1.42	1.29
F-Fractures	Lognormal	3.88	2.15

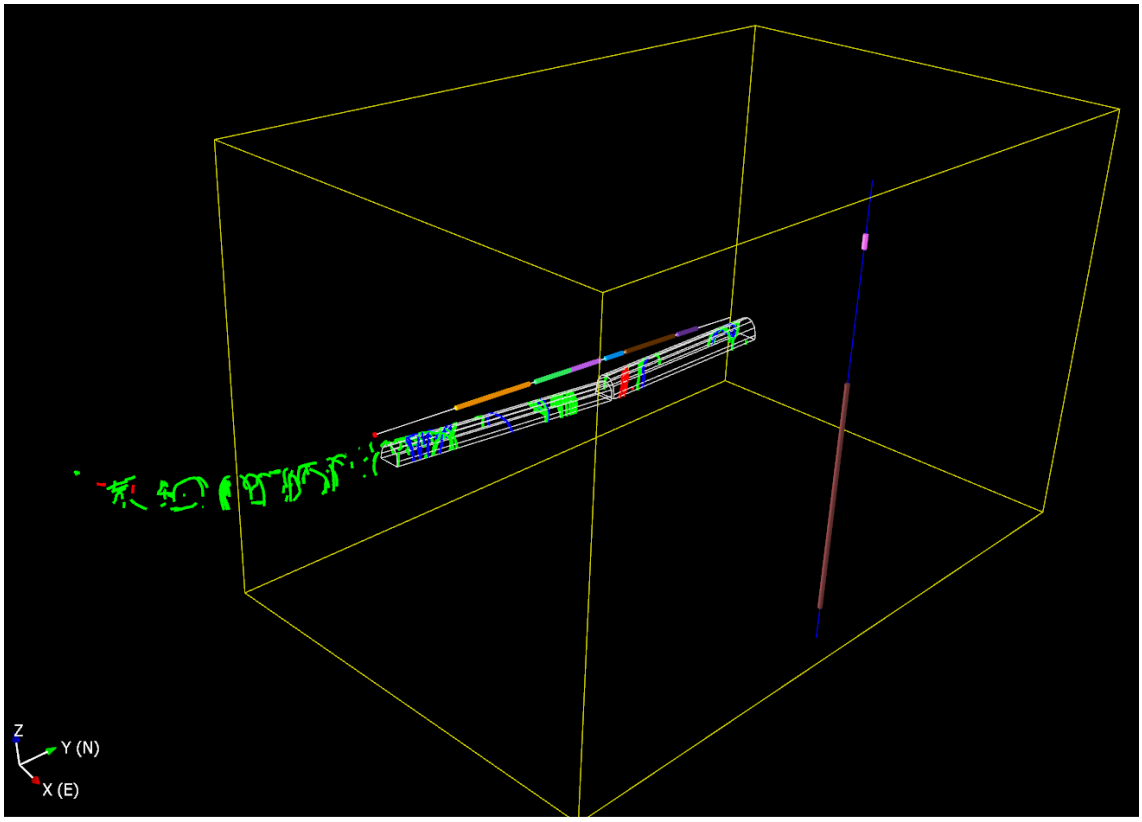

Note: F-fractures are shown in blue; D-fractures are shown in green; and -fractures are shown in red color.

Figure 4-2: Traces of the Fractures Included in the Analysis on the Research Tunnel Walls.

Fracture transmissivity can be estimated from the observed fracture flow using analytical solution for the unit inflow (Q) into a circular tunnel with radius r located at depth h (Ref. 4):

$$Q = \frac{2\pi k(A+H)}{\ln(\frac{h}{r}+\sqrt{\frac{h^2}{r^2}-1}} \quad , \qquad (4\text{-}1)$$

$$A = h(1-\alpha^2)/(1+\alpha^2) \text{ and } \alpha = \frac{1}{r}(h-\sqrt{h^2-r^2}\,,$$

where k is hydraulic conductivity.

The inflow through the fracture (Q_{fr}) with aperture b is:

$$Q_{fr} = Q \cdot b = \frac{2\pi T(A+H)}{\ln(\frac{h}{r}+\sqrt{\frac{h^2}{r^2}-1}}} \quad (4\text{-}2)$$

where T is fracture transmissivity.

From Eq. 4-2, the transmissivity of F fractures (Q_{fr} > 1.0 L/min) is > 3.2*10^{-8} m^2/s, transmissivity of D fractures (Q_{fr} < 0.1 L/min) is < 3.2*10^{-9} m^2/s, and the transmissivity of W fractures (Q_{fr}< 0.1 L/min*) is* < 3.2*10^{-9} m^2/s.

Table 4-3 shows the measured inflow into CTD and inclined drift and the inflow through the different fractures calculated assuming the following inflow rates: 2.3 L/min (F fractures), 0.23 L/min D fractures, and 0.1 L/min (W fractures). The calculated values are very close to the measured ones. Consequently, the transmissivity of F fractures is 7.3*10^{-8} m^2/s, transmissivity of D fractures is 7.3*10^{-9} m^2/s, and the transmissivity of W fractures is 3.2*10^{-9} m^2/s. Using the cubic law relationship (Ref. 5) between the transmissivity and aperture, the estimated aperture values are: 21 micron (F), 45 micron (D), and 16 micron (W).

Table 4-3. Comparison of Measured and Calculated Inflow into the Research Tunnel.

Research Tunnel Area	Measured Tunnel Inflow (L/min)	Number of Fractures			Calculated Fracture Flow (L/min)			
		F	D	W	F	D	W	Total
CTD	13	4	15	3	9.2	3.45	0.3	12.95
Inclined Drift	43	14	42	N/A	32.2	9.66	0	41.86

The estimates of the fracture parameters were used to derive the following relationships between the fracture permeability (k) and fracture radius (R) radius:

$$k[m^2] = 1.55 \cdot 10^{-12} \cdot R^{2.3} \quad (4\text{-}3)$$

The fractures in the research tunnel were generated then from the trace data. The dip direction and dip angle of the fractures were derived from the plane containing the fracture traces. The fracture radius was driven from the lognormal distributions (Table 4-2). The fracture permeability was correlated with the fracture radius using Eq. 4-3. Figure 4-3 shows the generated fractures.

Eq. 4-2 was used to calculate the inflow through each fracture (with fracture specific radius and permeability) shown in Figure 4-3. The results of these calculations are summarized in Table 4-4. The calculated inflow through generated fractures is in good agreement with the measured inflow into ythe research tunnel.

Table 4-4. Comparison of Calculated Inflow from Generated Fractures and Measured Inflow into Research Tunnel.

Generated Fractures		
Type	**∑ Transmissivity (m^2/s)**	**∑ Inflow (L/min)**
D	1.94E-06	61.03
F	1.58E-06	49.78
W	9.71E-08	3.06
Total	**3.62E-06**	**113.87**
Measured Inflow into the Research Tunnel (L/min): 104		

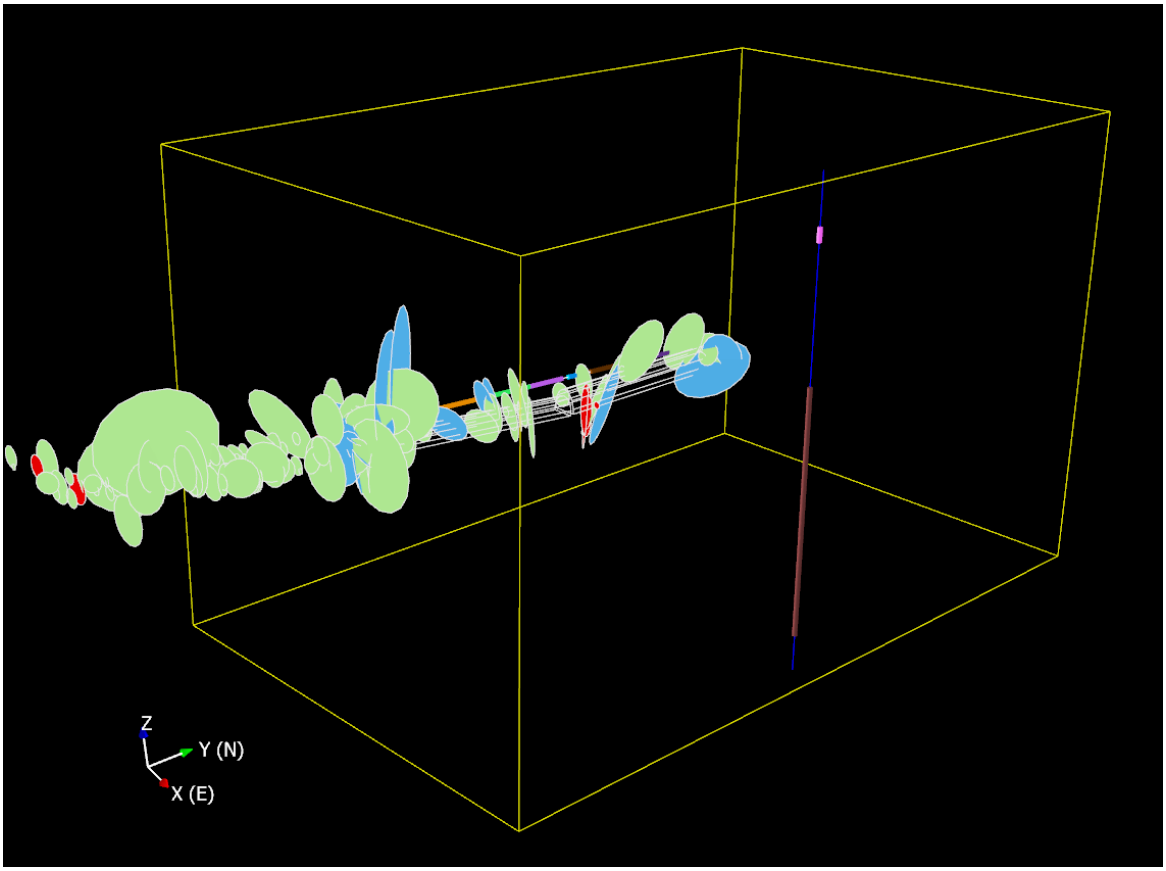

Note: F-fractures are shown in blue; D-fractures are shown in green; and -fractures are shown in red color.

Figure 4-3: Fracture Generated in the Research Tunnel.

4.3 GENERATING FRACTURES USING BOREHOLE 12MI33 FRACTURE DATA

Borehole 12MI33 is a horizontal borehole that is parallel to the Research tunnel (Figure 4-1). The packer tests were conducted in 6 test intervals. The test intervals also serve as the monitoring points for observation of temporal variations in pressure and geochemistry in vicinity of the Research tunnel.

297 fractures were recorded in the borehole. The fractures were classified as "crack"; "hair crack"; "discontinuity crack"; and "mineral vein". The fractures described as cracks that had recorded aperture values were assumed to be permeable fractures, such as F, D, and W fractures observed in the Research tunnel. 17 such fractures were identified. The fractures data were imported into the model. The fractures were generated in accordance with these data (depth and orientation) using F-fracture lognormal distribution for fracture radius. F-fracture radius distribution produced closer results to the packer test results as shown below. The fractures generated in the borehole are shown in Figure 4-4 along with the Research tunnel fractures. Figure 4-4 also shows the transmissivity of the test intervals obtained in the packer tests. The high transmissivity intervals 1, 2' and 6 coincide with the zones in which fractures generated in both, Research tunnel and borehole are present. Intervals 2 and 3 intersect a few fractures and their transmissivity is lower. Intervals 4 and 5 do not intersect any of generated fractures and their transmissivity is significantly lower.

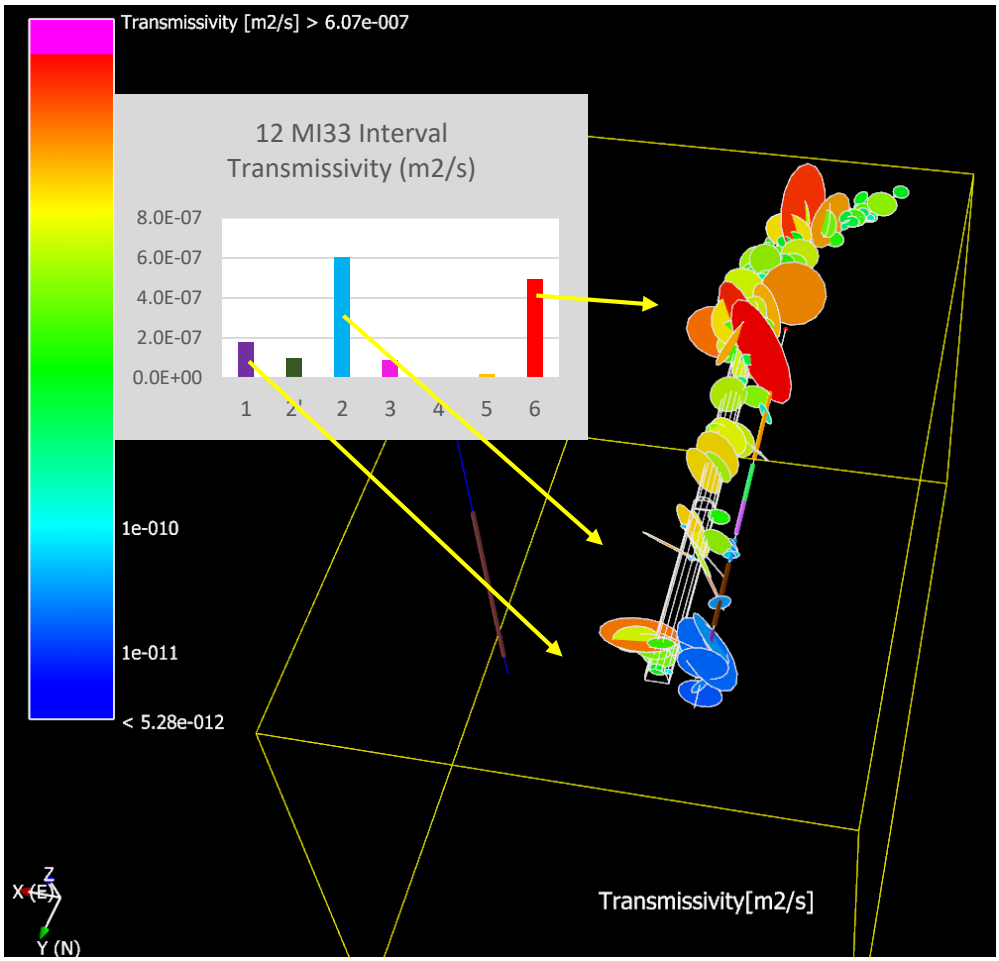

Figure 4-4: Transmissivity of Fractures in the Research Tunnel and Borehole 12MI33.

Tables 4-5 and 4-6 compare the transmissivity of the generated fractures in borehole 12MI33 and the transmissivity of the test intervals from the packer tests in this borehole. The total transmissivity of fractures generated in the borehole ($7.6x10^{-7}$ m^2/s) is close to the total transmissivity of the test intervals ($9.9x10^{-7}$ m^2/s).

Table 4-5. Transmissivity of the Generated fractures in Borehole 12MI33

Fracture	Transmissivity (m^2/s)	Fracture	Transmissivity (m^2/s)
1	1.14E-08	10	8.30E-09
2	2.71E-09	11	5.36E-09
3	1.74E-08	12	2.62E-09
4	7.26E-09	13	1.60E-08
5	1.39E-08	14	2.34E-08
6	2.94E-09	**15**	4.27E-07
7	6.28E-08	**16**	6.59E-08
8	5.01E-08	**17**	1.82E-08
9	2.30E-08	**Total**	**7.58E-07**

Table 4-6. Transmissivity of the Test Intervals from Borehole 12Mi33 Packer Tests.

Interval	Transmissivity (m^2/s)
1	1.78E-07
2'	9.78E-08
2	6.01E-07
3	8.65E-08
4	4.96E-09
5	1.93E-08
6	4.91E-07
Total	**9.88E-07**

4.4 GENERATING STOCHASTIC FRACTURES IN THE MODELING DOMAIN

The following input data are needed to generate stochastic fractures in the modeling domain:

- number of fracture sets
- orientation distribution of each set
- fracture intensity in each set

The number of fracture sets and their orientation was obtained from the analysis of the fractures generated from the tunnel traces using Fracman tool Interactive Set Identification System (ISIS). ISIS defines fracture sets from field data using an adaptive probabilistic pattern recognition algorithm. ISIS calculates the distribution of orientations for the fractures assigned to each set, and then reassigns fractures to sets according to probabilistic weights proportional to their similarity to other fractures in the set. The orientations of the sets are then recalculated and the process is repeated until the set assignment is optimized.

Based on ISIS analysis (Figure 4-5) it was concluded that all the fractures, except the ones in the inclined drift, belong to one set that is best described by Fisher distribution with mean pole 208^0 (local coordinate system rotated 10.2^0 clockwise in x-y plane to align the tunnel along the y axis) mean plunge 8^0 and the concentration parameter k equal to 7. An additional fracture can be identified in the inclined drift. However, this set is not considered because the inclined drift is located outside the modeling domain. It likely that the conditions around the inclined drift are affected by located in close vicinity Main-shaft fault and the upper highly fractured domain (UHFD).

Fracture intensity has direct impact on how many fractures will be generated in the modeling domain. Fracture intensity can be specified either as number of fractures in the set (not recommended because it is scale dependent) or as volumetric intensity of fractures in the set, also known as P_{32}. P_{32} [1/m] is scale independent and represents fracture area per unit volume of rock. Neither number of fractures or P_{32} can be directly measured.

This analysis uses the observed linear intensity P_{10} (number of fractures per unit length) of fractures in the tunnel (0.19 fractures/m) and in the borehole 12MI33 (0.17 fractures/m) to evaluate P_{32}. The stochastic fractures are generated using Fisher distribution described above, fracture radius (Table 4-2), and fracture permeability (Eq. 4-3). The fracture P_{32} value is iteratively redefined until the P_{10} values in 2 arbitrary placed imaginary horizontal boreholes matches P_{10} of fractures observed in the tunnel and 12MI33. Figure 6 shows the stochastic fractures intersected by the two imaginary horizontal boreholes with P_{32}=0.22 1/m. The P_{10} in both boreholes (0.19 fractures/m) matches the observed P_{10} in the tunnel and is very close to the observed P_{10} in 12MI22.

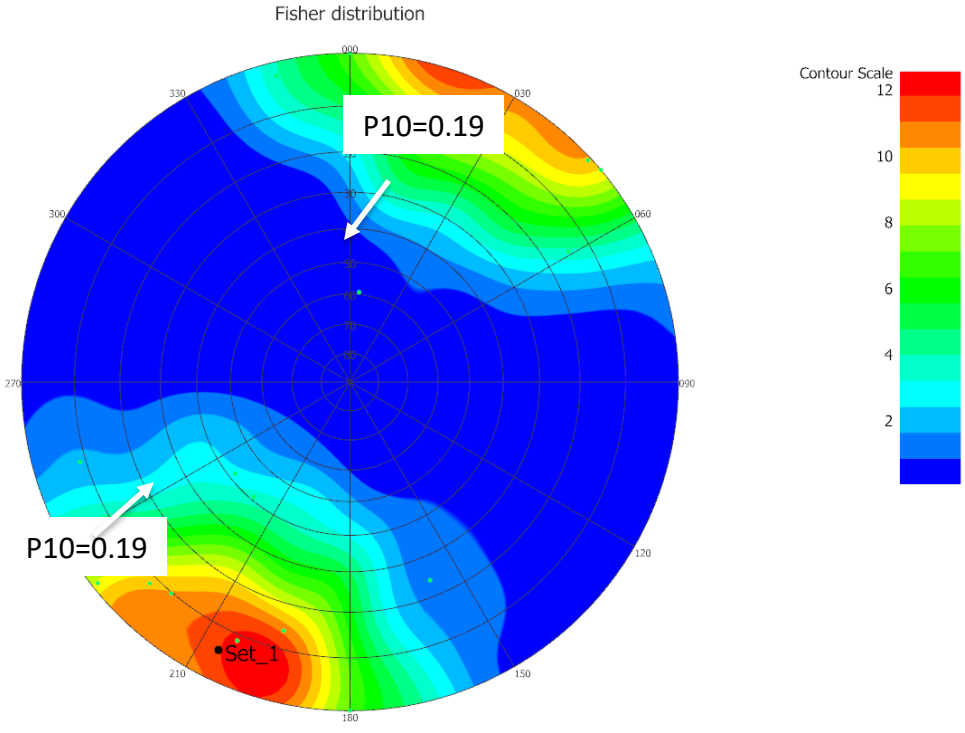

Figure 4-5: Fracture Set Identified by ISIS Analysis.

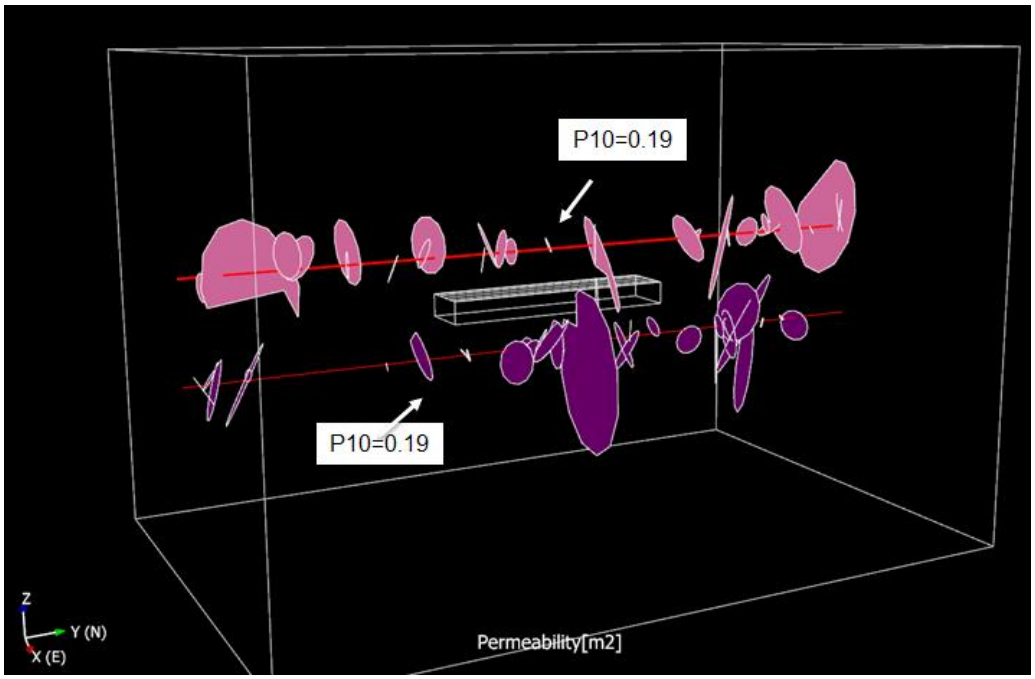

Figure 4-6: Stochastic Fractures Intersecting Two Imaginary Horizontal Boreholes.

The significantly lower P_{10} values (0.04) were calculated for two arbitrarily placed vertical boreholes (Figure 4-7). This is because vertical borehole has lower probability of intersecting sub-vertical fractures.

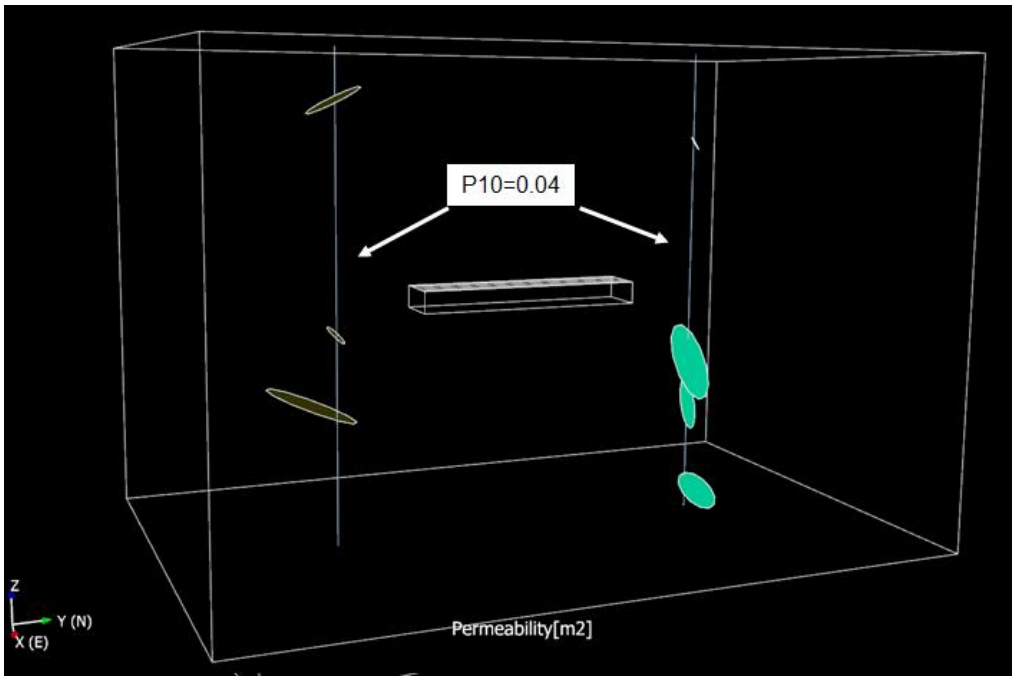

Figure 4-7: Stochastic Fractures Intersecting Two Imaginary Vertical Boreholes.

4.5 COMPARISON TO THE PACKER TEST RESULTS IN BOREHOLE MIZ-1

Figure 4-8 shows the stochastic fractures that intersect upper and lower test intervals of the vertical borehole MIZ-1. The transmissivity of the generated fractures is provided in Table 4-7. The packer test results are summarized in Table 8. The total transmissivity of fractures is higher than the total transmissivity obtained in the packer tests. The horizontal flow to the vertical borehole in the packer tests is affected by the horizontal permeability. The horizontal permeability is lower than vertical because the fractures are sub-vertical. This can explain the difference. Also, only one realization was used in this comparison.

Table 4-7. Transmissivity of Stochastic Fractures Intersected by Borehole MIZ-1.

Fracture	Transmissivity (m^2/s)
1	9.54E-08
2	3.54E-08
3	7.34E-09
4	2.52E-08
5	4.38E-08
Total	**2.07E-07**

Table 4-8. Packer Test Results in Borehole 12MI33.

Interval		Transmissivity (m^2/s)
Top (m)	**Bottom, m**	
-260.4	-263.3	3.69-08
-290.9	-342.4	5.16-09
Total		**4.20-08**

NOTE: Only the test intervals within the modeling domain are considered.

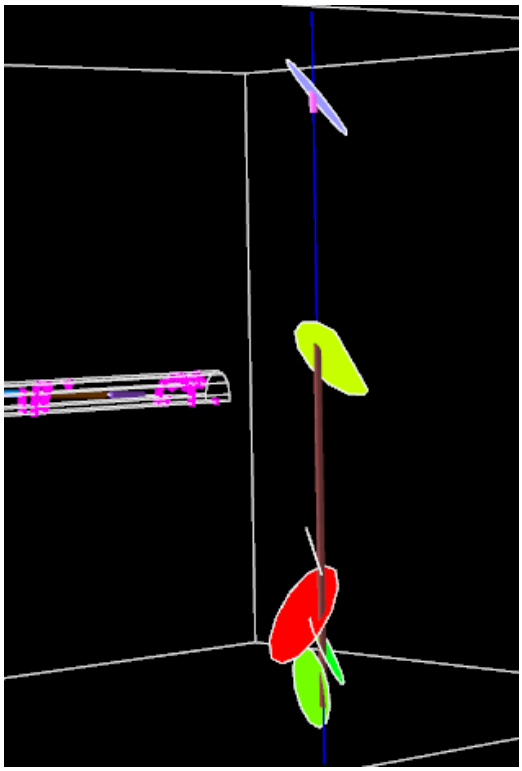

Figure 4-8. Stochastic Fractures Intersected by Borehole MIZ-1.

Figure 4-9 shows one realization of the stochastic fractures generated in the modeling domain. The color scale is used to show fracture transmissivity. Note that stochastic fractures are removed from the region surrounding the CTD, inclined drift, and borehole 12MI33. The fractures in this region are the ones shown in Figure 4-4.

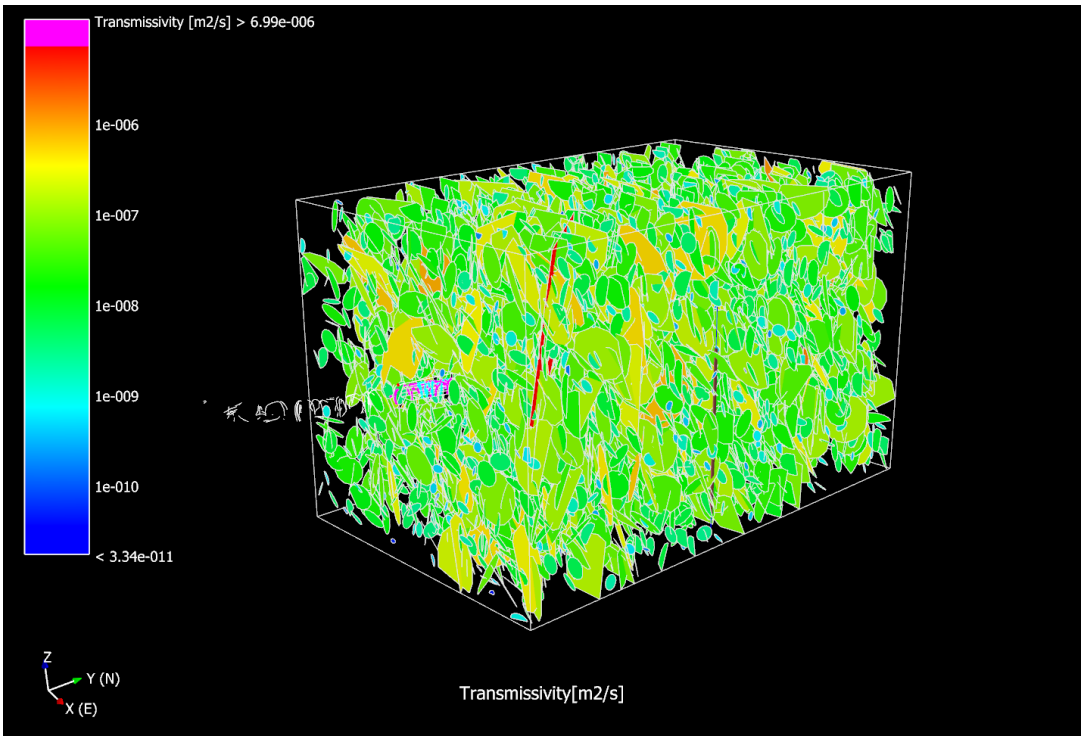

Figure 4-9: One Realization of the Stochastic Fractures Generated in the Modeling Domain.

4.6 CONVERTING DFN INTO THE EQUIVALENT CONTINUUM MODEL

After the DFN is generated, it can be converted to an effective continuum model using Oda's method. Oda's method calculates permeability tensors in three dimensions for each cell. Oda tensor is a simplification of Darcy's Law for flow through an isotropic porous medium. The fracture permeability (k) is projected onto the plane of the fracture and scaled by the ratio between the fracture volume (porosity) and the volume of the grid cell. The method is implemented in Fracman in accordance with the following equation (Ref. 1):

$$k_{i,j} = \frac{1}{12}(F_{k,k}\delta_{i,j} - F_{i,j}) \qquad (4\text{-}4)$$

$$F_{i,j} = \frac{1}{V}\sum_{k=1}^{N} A_k T_k n_{i,k} n_{j,k}$$

where $k_{i,j}$ is permeability tensor; $\delta_{i,j}$ is Kroenecker's delta; $F_{i,j}$ is fracture tensor; V is grid cell volume; N is total number of fractures in grid cell; A_k is area of fracture k; T_k is transmissivity of fracture k; and $n_{i,k}$, $n_{j,k}$ are the components of a unit normal to the fracture k. Note that only principle components of the permeability tensor (K_{xx}, K_{yy}, and K_{zz}) are the inputs into the flow and transport model.

Fracture porosity (ϵ) of the grid cell is calculated as:

$$\epsilon = \frac{1}{V}\sum_{k=1}^{N} A_k b_k \qquad (4\text{-}5)$$

where b_k is the aperture of fracture k.

The permeability and porosity of the grid cells without fractures can be defined in accordance with the matrix permeability and porosity. Figure 4-10 shows the grid cell permeability (K_{xx}) of the DFN realization shown in Figure 4-9. Figure 11 shows the vertical slice through CTD and Inclined drift.

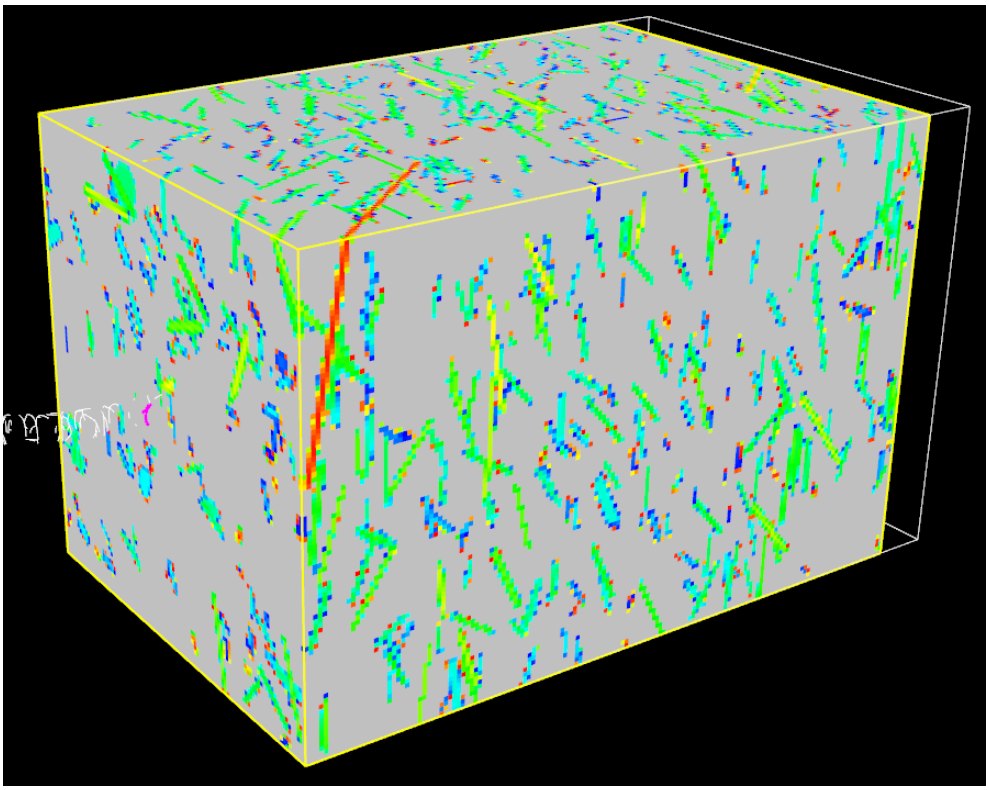

Figure 4-10: Grid Cell Permeability for DFN Realization Shown in Figure 9.

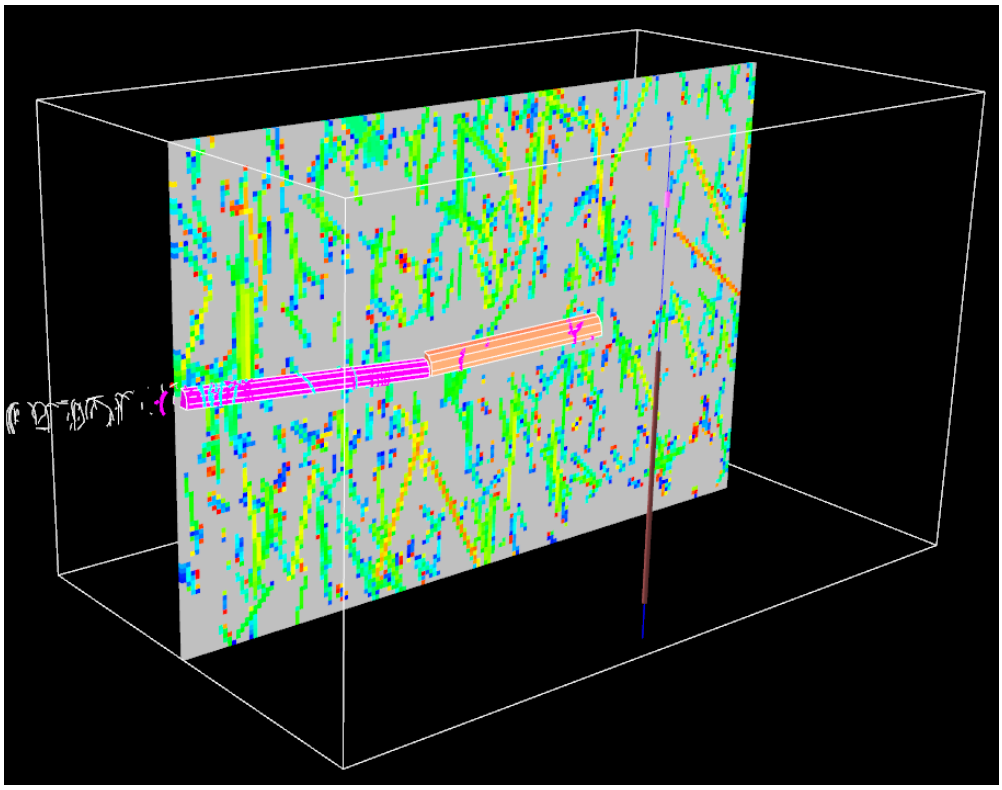

Figure 4-11: Vertical Slice of Grid Cell Permeability for DFN Realization Shown in Figure 9.

Table 4-9 summarizes the mean properties of the grid cells in the modeling domain. The calculated mean permeability values are close to suggested reference permeability (1E-15 m^2). However, the permeability is anisotropic and changes over a few orders of magnitudes.

Table 4-9. Effective Continuum Model Mean Grid Cell Properties.

Parameter	Notation	Mean Value
Permeability (m^2)	K_{xx}	3.52E-15
	K_{yy}	2.50E-15
	K_{zz}	4.78E-15
Anisotropy	K_{xx}/K_{zz}	0.73
	K_{yy}/K_{zz}	0.52
	K_{yy}/K_{xx}	0.71
Fracture Porosity	€	1.65E-05

4.7 SUMMARY

Analysis of fractures in the research tunnel and borehole 12MI33 allowed for estimating fracture size, orientation and permeability. This information was used to generate stochastic fractures in the modeling domain. The volumetric fracture intensity was estimated by matching the linear fracture intensity of the generated stochastic fractures with the observed linear fracture intensity. The obtained fracture properties were used to generate DFN model. The DFN was converted to the effective continuum model using Oda's method. One realization of DFN was used as an example. Multiple realizations will be generated using this method for the analysis of flow and transport conditions in and around the research tunnel.

4.8 REFERENCES

1. Golder Associates, Inc. (2017). *Interactive Discrete Feature Data Analysis, Geometric Modeling and Exploration Simulation*, FracMan Manual, April 6, 2017.

2. Zhang, H.H. Einstein and Dershowitz, W.S. (2002). *Stereological relationship between trace length and size distribution of elliptical discontinuities*, Geotechnique, 52/6 (2002), pp. 419-433.

3. La Pointe, R.P. (2002). *Derivation of parent fracture population statistics from trace length measurements of fractal fracture populations*, International Journal of Rock Mechanics & Mining Sciences, 39 (2002), pp. 381–388.

4. Butscher, C. (2012). *Steady-State Groundwater Inflow into a Circular Tunnel*, Tunnelling and Underground Space Technology, 32 (2012), pp. 158–167.

5. Snow, D. (1969). *Anisotropic Permeability of Fractured Media*, Water Resources Research, 5 1969), pp. 1273–1289.

5. SUMMARY

SNL has been participating in three tasks of the DECOVALEX project: Task A. Modeling gas injection experiments (ENGINEER), Task C. Modeling groundwater recovery experiment in tunnel (GREET), and Task F. Fluid inclusion and movement in the tight rock (FINITO). The major accomplishments are summarized below:

- *Task A. Modeling gas injection experiments (ENGINEER):* Bentonite has been proposed as a buffer material for a deep geologic repository. Understanding gas migration in compacted clay materials is important for a performance assessment of an engineered barrier system of a repository system. Existing data demonstrate the complexity of gas migration in such low-permeability materials. Through a simple model analysis, we here show that this complexity can probably be explained with a bifurcation and chaos concept. The dynamic behavior of the system has been shown closely related to clay matrix dilation, fracturing and fracture healing as induced by gas bubble movement. The concept proposed here provide a new perspective for modeling gas migration in low-permeability materials.
- *Task C. Modeling groundwater recovery experiment in tunnel (GREET):* The task uses the data collected in a research tunnel at 500 m depth, at the Japan Atomic Energy Agency (JAEA) Mizunami Underground Research Laboratory (MIU), to understand the hydrological-mechanical-chemical environment. One of the objectives of Task C, Step 1, is to establish modeling methods and tools for analysis of excavation of tunnel. Fracture data analysis and preliminary modeling analysis have been carried out at SNL as part of Task C, Step 1. The fracture data analysis utilizes fracture data collected in the research tunnel and monitoring borehole 12MI33. A discrete fracture model has been developed based on fracture orientation, size and intensity derived from the fracture data analysis. The discrete model has been upscaled to an effective continuum model to be used in flow and transport simulations. A preliminary modeling analysis has also used project data to construct a simulation model to predict inflow into the inclined drift and the Closure Test Drift (CTD) during excavation.
- *Task F. Fluid inclusion and movement in the tight rock (FINITO):* Fluid inclusions can be found within mineral crystals or along grain boundaries in all types of sedimentary rocks. For a long-term performance assessment of a geologic repository, it is important to characterize the distribution, amount and interconnectivity of fluid inclusions in the host rock and to predict migration of these inclusions after waste emplacement. Task F is designed to gain mechanistic understanding of possible physical processes involved in fluid inclusion migration in tight rocks such as rock salt or shale, with an ultimate goal to develop robust, predictive THMC modeling tools for a long-term performance assessment of a deep geologic repository in such media. The task will leverage the data provided by BGR, Germany. In fiscal year 2017, the work at SNL has focused on the model formulation of an individual fluid inclusion in rock salt. The model developed can qualitatively explain a number of key features of experimental observations. Specifically, the model can predict: (1) a linear increase in migration evelocity with increasing thermal gradient, (2) a nonlinear increase in migration velocity with inclusion size, (3) an overall aceleration in fluid migration with temperature, (4) the dependence of migration velocity on mechanical loadings. A preliminary analysis for biphase fluid inclusions has also been

performed. A bifurcation point in vapor/liquid volume ratio for the direction of fluid migration is derived.